

DISSERTATION

SPIN MULTIPLETS: THEORY AND APPLICATION

Submitted by

Jacob M. Nite

Department of Chemistry

In partial fulfillment of the requirements

For the Degree of Doctor of Philosophy

Colorado State University

Fort Collins, Colorado

Spring 2018

Doctoral Committee:

Advisor: Anthony K. Rappé

Matthew Shores

Yian Shi

Siu Au Lee

Copyright by Jacob Matthew Nite 2018

All Rights Reserved

ABSTRACT

SPIN MULTIPLETS: THEORY AND APPLICATION

Transition metal complexes have seen an increased use as photocatalysts for organic reactions in recent literature, mostly involving the Ru(II)(bpy)₃ family of catalysts. Due to the rarity of ruthenium in the Earth's crust, alternative catalysts using Earth abundant materials are desirable. Recent literature has shown that chromium based catalysts show great promise as a replacement for ruthenium for some reactions. The mechanisms of these first-row transition metal complexes are significantly more complex than those of the second and third row. The excited state complexities of first-row transition metal complexes are challenges for both experimental and theoretical research. The complexities of the excited states require theoretical methods beyond the standard single reference methods commonly used in the literature. Through the use of recent multi-reference post Hartree Fock (HF) methods as well as a new multi-reference density functional theory (DFT), insights into the character of chromium-based photocatalysts were examined.

A new multi-determinant DFT method named few-determinant density functional theory (FD-DFT) was described. FD-DFT incorporates multiple DFT determinants using a finite difference approach to calculate the exchanges between multiple determinants for open shell multiplets. The method is implemented in a generalized bond valence (GVB) wave function, and can be converged through an SCF procedure. The system was benchmarked using oxygen atom and diatomic oxygen as well as atomic systems

with more open shell orbitals. The benchmarking shows stability across many different functional choices, and gives good excitation energies with and without SCF convergence.

The Cr(III)(AcAc)₃ system has been long studied for its unique excited state properties that defy the standard cascade model for excited state relaxation. The tris(1,3-propanedionato)chromium(III) (Cr(III)(PDO)₃) complex was studied as an analog to the Cr(III)(AcAc)₃ system to understand the excited state pathway between the initial excited ⁴T_{2g} state and the long lived ²E_g state. Using the FD-DFT method as well as the multi-reference spectroscopy oriented configuration interaction (SORCI) method, the initial excited state energies were studied compared to previous perturbation theory (PT) approaches. Both SORCI and FD-DFT calculate reasonable ²E_g excitation energies, an improvement over earlier results. The SORCI method was also used to map the potential energy curve between the initial ⁴T_{2g} excited state and its fully relaxed distorted structure. The pathway agrees with previous experimental and theoretical studies showing that a transitionless path exists between the quartet and doublet states, but spin-orbit coupling calculations suggest that a direct path between the ⁴T_{2g} and ²E_g is possible rather than needing an internal conversion step to the lowest ²E_g state.

Chromium-based photocatalysts have been recently studied in the literature as having a competitive mechanism between the reaction substrate and O₂ whereby the O₂ quenches the excited catalyst. Using the combined Cr(III)(PDO)₃ • O₂ system, the likely states by which this quenching event occurs were studied with FD-DFT as well as recent multi-reference PT approaches. Comparing the excited state calculated using the multi-reference based methods to standard DFT calculations shows the inability of

single-determinant methods to correctly produce the proper excited state character even when obtaining somewhat reasonable energies. The excited state responsible for the quenching of the excited complex is identified using spin density plots of the CASSCF calculations.

The search for suitable first-row transition metals requires a search across possible ligands and metal centers. Using the success of chromium-based catalysts, isoelectronic vanadium catalysts were studied to identify any potential differences between the complexes as well as identify the utility of vanadium-based catalysts. Using a variety of methods, including TDDFT-based absorption spectra, vibrational component plots of the excited state distortions, and SORCI potential energy curves (PEC), the differences between the chromium and vanadium catalysts were examined. It was found that vanadium catalysts absorptions are shifted significantly from chromium complexes and the vanadium excited states disperse the unpaired electron over the complex instead of localizing it on the metal center. The distortions in the chromium-based catalysts have a greater amount of asymmetric vibrational character compared to vanadium, which shows mostly symmetric behavior. Lastly, the SORCI PECs show that, unlike chromium, the doublet curves do not intersect the quartet curves, making a transition to a long lived doublet state a significantly slower process. The results highlight significant differences between the complexes even with ligand structure is controlled.

ACKNOWLEDGEMENTS

Graduate school has been a journey that has shaped me as a scientist in ways that could have not been foreseen at the start. While the work I have accomplished has been mine, my achievements have been built upon the people who have supported me in my endeavors.

I want thank Anthony Rappé, my advisor, for the tremendous guidance he has provided me during my graduate work. The most important lesson he has taught me is that the cutting edge of science is not always the most complicated problems, but instead it is in determining the relative sizes of each piece within any problem and what you can do to understand which has largest impact. He also has shown me that your ego can only make your science worse, so there isn't a point to having one.

I want to thank my committee, Matthew Shores, Yian Shi, and Siu Au Lee. They have been indispensable in their encouragement for me to finish my PhD. They have taught me to look beyond my expertise and see how it fits into the rest of the science community.

I would like to the chemistry faculty, specifically Melissa Reynolds and Nancy Levinger. They have always been students biggest supporters, and have not hesitated to put students before politics. They have been there to help me navigate graduate school even when my personal life was hectic.

I want to acknowledge my family, especially my parents for always encouraging me to stick with my PhD program and finish. They always believed that I could finish my degree even when life gets busy.

I want to thank my wife's family, especially Stacy Dutton. She has been a great source of encouragement for my work, and has been one of my biggest cheerleaders as a scientist and a father. She is always willing to drop everything to come help when she is needed.

I want to thank my friends for the rest and relaxation you provided. Graduate school is a long journey. Everyone in it needs to pace themselves and take a break once in a while.

I want to thank my children, Augustine and Elisabeth. Daddy is eternally grateful that you slept at night long enough for him to finish this dissertation.

Most of all, I want to thank my lovely wife, Collette, for helping me be the best scientist, husband, and father I can be. When I was down, you helped me; when I was frustrated, you encouraged me; when I was joyful, you laughed with me; when I was worried, you consoled me; when I was exploring new adventures; you supported me. I owe everything to you, including my science, and I cannot fully express my gratitude for you being in my life.

DEDICATION

To my wife, Collette, for believing in me.

TABLE OF CONTENTS

ABSTRACT	ii
ACKNOWLEDGEMENTS.....	v
DEDICATION	vii
LIST OF TABLES	x
LIST OF FIGURES	xi
CHAPTER 1: INTRODUCTION.....	1
BACKGROUND:.....	1
SPECIFIC AIMS OF THIS RESEARCH:	13
REFERENCES	15
CHAPTER 2: FEW-DETERMINANT DENSITY FUNCTIONAL THEORY (FD-DFT), SPIN MULTIPLTS AS PROOF OF CONCEPT.....	18
INTRODUCTION:	18
THEORY:.....	19
FD-DFT THEORY:	19
GVB IMPLEMENTATION:.....	25
APPLICATIONS:.....	28
THEORETICAL BENCHMARKING:.....	28
ATOMIC AND MOLECULAR OXYGEN:	28
THREE ELECTRON SYSTEMS, NITROGEN ATOM AND Cr(III) ION:.....	32
FIVE ELECTRON SYSTEMS Fe(III):.....	35
CONCLUSIONS:	36
REFERENCES	39
CHAPTER 3: TRIS(1,3-PROPANEDIONATO)CHROMIUM(III) FOR INSIGHT INTO Cr(III) BASED PHOTOCATALYSTS	43
INTRODUCTION:	43
COMPUTATIONAL METHODS:.....	47
STRUCTURE OPTIMIZATIONS:	47
REACTION PATHWAY:.....	48
FD-DFT CI:.....	48
SORCI:.....	49
RESULTS:	50
CONCLUSIONS:	54
REFERENCES	55
CHAPTER 4: UNDERSTANDING Cr(III) PHOTOCATALYSTS QUENCHING BY O ₂ ...	58
INTRODUCTION:	58
COMPUTATIONAL METHODS:.....	60
RESULTS:	61
CONCLUSIONS:	66
REFERENCES	67
CHAPTER 5: COMPARISON OF EXCITED STATE PROPERTIES OF CHROMIUM(III) AND VANADIUM(II) COMPLEXES: POTENTIAL AS PHOTOCATALYSTS.....	69
INTRODUCTION:	69

THEORETICAL METHODS:.....	71
STRUCTURE OPTIMIZATION AND THEORETICAL SPECTRA:.....	71
Cr / V(PDO) ₃ :.....	72
VIBRATIONAL PROJECTIONS:	73
RESULTS & DISCUSSION:	74
TDDFT:.....	74
SPIN DENSITY PLOTS:.....	75
VIBRATIONAL PROJECTION SPECTRA:	80
SORCI:.....	82
CONCLUSIONS:	84
REFERENCES.....	86
CHAPTER 6: FUTURE DIRECTIONS.....	87
APPENDIX A: BROKEN SYMMETRY WAVEFUNCTIONS.....	89
REFERENCES.....	95
APPENDIX B: FD-DFT INTERDETERMINANT DFT EXCHANGE ENERGY FOR FOUR OPEN SHELL ORBITALS	96

LIST OF TABLES

Table 2.1: O and O ₂ excitation energies.....	31
Table 2.2: Excitation energies for nitrogen atom.....	34
Table 2.3: Cr(III) ion excitation energies for the ⁴ F to ² G transition.....	34
Table 2.4: Fe(III) ion excitation energies for the quartet transition.....	37
Table 3.1: Excitation energies for the ⁴ A _{2g} geometry for the AcAc and PDO ligands.....	51
Table 4.1: Cr(III)(PDO) ₃ • O ₂ excitation energy comparison.....	62
Table 5.1: Spin density plots of quartet and doublets states of the Cr(III)bpy ₃ and V(II)bpy ₃ photocomplexes.....	77
Table 5.2: Spin density plots of quartet and doublets states of the Cr(III)pod and V(II)pod photocomplexes.....	78
Table 5.3: Spin density plots of quartet and doublets states of the Cr(III)esterpod and V(II)esterpod photocomplexes.....	79

LIST OF FIGURES

Figure 2.1: Electronic configuration for O ₂ ground and excited states	29
Figure 3.1: SORCI calculations for the linear reaction path	52
Figure 3.2: SORCI excited state calculations including SOC contributions	53
Figure 4.1: Reaction scheme for the quenching of chromium (III)	59
Figure 4.2: Spin density plots for the Heisenberg ladder states for Cr(III)(PDO) ₃ • O ₂ ...	63
Figure 4.3: Spin density plots for the excited quartet states for Cr(III)(PDO) ₃ • O ₂	65
Figure 5.1: TDDFT(APF-D/6-311+G*) spectra of various first row transition metal Schiff base complexes.	74
Figure 5.2: TDDFT(APF-D/6-311+G*) spectra of various first row transition metal salen type complexes.	75
Figure 5.3: Vibrational distortion projection plot	81
Figure 5.4: Plot of excited state energies of X(PDO) ₃ complexes	83
Figure A.1: H ₂ dissociation curve in terms of total energy.....	93
Figure A.2: H ₂ molecule total energy as a function of overlap.....	94

CHAPTER 1: INTRODUCTION

BACKGROUND:

Green chemistry has seen increased interest, and a substantial effort has focused on the development of new catalysts. Photocatalysts fulfill the green chemistry ideals to a large extent, since light energy is harnessed rather than heat as a reaction driving force, catalysis leads to reagent reduction, and potential auxiliary agent elimination also contributes to waste reduction. An interesting class of photocatalysts that have seen increased attention in the literature are transition metal photocatalysis. Specifically, the work done on tris(bipyridine)ruthenium(II) (Ru(II)(bpy)_3) and its derivatives have been implemented to catalyze a large variety of classic organic reactions with visible light, effectively ushering a new green chemistry avenue.

Ru(II)(bpy)_3 has been known to catalyze organic reactions since the 1980s with the initial work done by Cano-Yelo and Deronzier, but interest in the field shifted to electrochemical approaches.¹ In the late 2000s, the use of Ru(II)(bpy)_3 as a catalyst was reinvigorated and caught wide attention. Since then, it has been applied to a large variety of reactions including Diels-Alder cycloadditions, dehalogenations, oxidations of alcohols, as well many others.²⁻⁷ The real advantage that Ru(II) based catalysts have is that the diversity of possible reactions only requires a few catalysts. This is compounded by the ability of Ru(II)(bpy)_3 to undergo both oxidative and reductive catalyzing pathways.² In addition, Ru(II)(bpy)_3 -like catalysts absorb in the visible reaction, making it possible to use cheap irradiation sources for the synthesis.

While the advantages of Ru(II)- and Ir(III)-based catalysts are numerous, they share one large disadvantage with respect to their natural abundance. The natural abundance of ruthenium metal is nine orders of magnitude less than that of silicon and iridium itself is two orders of magnitude rarer than ruthenium.⁸ This is a huge concern when attempting to scale these reactions to industrial levels because the cost of the catalyst plays a large role in the overall economics of the reaction. Having a total cost lower than current methods gives a large incentive to switch to using greener methods on a large scale, though novel reactivity is a powerful incentive as well.

Switching the metal center from ruthenium and iridium to a first row transition metal would appear to be the solution to the problem of elemental scarcity since first row transition metals are several orders of magnitude more abundant than their second and third row counterparts.⁸ First-row transition metals exhibit significantly different properties in complexes than metals in the same period. For example, Fe(II) and Ru(II) are both d^6 metals, but Ru(II) is always low spin and Fe(II) is either high or low spin depending the ligands complexed to the metal. This requires much more care in ligand and metal choice when developing a suitable photocatalysts.

Recent examples in the literature have shown promise in developing photocatalysts using first row transition metals. Stevenson et al. used a Cr(III)(Ph₂phen)₃ complex to catalyze a series of Diels-Alder reactions.⁹ This catalyst was found to proceed through a mechanism which is stoichiometric in photons whereas the mechanisms using ruthenium based catalysts proceed via radical chain initiation.¹⁰

The work on chromium-based catalysts as an alternative to ruthenium-based complexes highlights the challenges presented by first-row based photocatalysts. While

it is advantageous to have catalysts that exhibit different properties from the ruthenium catalysts, they require effort analyzing many possible mechanistic pathways to determine how one particular catalyst works for a given reaction and learn of the pathways can be generalized. As shown in the work by Higgins et al in understanding the Cr(III)(Ph₂phen) photocatalyst's role for a Diels-Alder mechanism, theory can play an important role in unraveling these mechanism pathways.¹⁰

Theory can accelerate the replacement of ruthenium with first row transition metals in photocatalysts in two major areas: the catalyst's role in mechanisms that have been discovered experimentally, and proposing new catalysts that share theoretical properties with those that function experimentally. For both of the these areas, accurate energies are needed for the transitions between the ground state and the relevant excited states as well as the structures of the excited states if complexes undergo geometry changes upon excitation. The theoretical excitation and emission energies give an estimate of the oxidation or reduction potential of a photocatalyst.¹⁰ In addition, the molecular orbitals and spin density plots can give a picture of whether or not a particular catalyst can act as a oxidizing or reducing agent in the reaction by knowing where the electron is in a given excited state. This gives some tools to understand details about these reactions that are difficult or impossible to measure experimentally.

Transition metal complexes and their excited states present significant theoretical challenges that must be addressed in order to obtain useful energies and therefore other properties from these systems. Transition metals themselves are more computationally difficult than the traditional organic atoms. The presence of partially filled d orbital shells complicate the calculations not only due to the extra unpaired

electrons but also the potential for high- and low-spin configurations. The relative d orbital energy levels are also sensitive to the ligand nature and solvent environment. Replicating the exact solvent environment can be complicated since both implicit and explicit solvent may be needed, which can change the electron configuration for many first-row transition metal complexes. Larger complexes more representative of experimentally useful catalysts can have large, extended ligand structures that can interact with several different substrates during a single mechanistic pathway, making theoretical studies computationally burdensome. Many different computational approaches can be applied to these systems, each with their individual advantages.¹¹

The theoretical methods used to study the photophysics and photochemistry of first-row transition metal complexes must be able to properly model the excited states, so that accurate excitation energies can be obtained and the characteristics of the excited states in terms of the molecular orbitals and spin densities are representative of the excited states. For complexes useful in photocatalytic applications, the excited states often consist of spin states that cannot be described by a single Slater determinant. While the ground states and some of the excited states are representable by a single determinant, many of the important excited states consist of at least two determinants. Slater determinants encapsulate the antisymmetric nature of electronic wave functions. A three electron $M_s = \frac{1}{2}$ Slater determinant and its determinantal expansion is provided in Eq. (1.1).

In Eq. (1.1) ϕ_a is a one electron spatial orbital, α denotes the spin, and (1) indicates that is electron 1. The three-electron quartet ground state can be described by the determinantal expansion of $\phi_a\alpha(1)\phi_a\alpha(2)\phi_a\alpha(3)$, but the lowest doublet requires

$\phi_a\alpha(1)\phi_a\beta(2)\phi_a\alpha(3) - \phi_a\beta(1)\phi_a\alpha(2)\phi_a\alpha(3)$ in order to be a proper spin-eigenfunction. Many of the staple theoretical tools such as Hartree Fock (HF) and density functional theory (DFT) cannot describe these states to an accurate level, which can result in excitation energies being several electron volts in error. The rigorous solution to this problem is to use wave function methods that are defined in terms of multiple determinants.

$$\begin{aligned} & \begin{vmatrix} \phi_a\alpha(1) & \phi_a\alpha(2) & \phi_a\alpha(3) \\ \phi_b\beta(1) & \phi_b\beta(2) & \phi_b\beta(3) \\ \phi_c\alpha(1) & \phi_c\alpha(2) & \phi_c\alpha(3) \end{vmatrix} = \\ & \phi_a\alpha(1)(\phi_b\beta(2)\phi_c\alpha(3) - \phi_c\alpha(2)\phi_b\beta(3)) \\ & - \phi_b\beta(1)(\phi_a\alpha(2)\phi_c\alpha(3) - \phi_c\alpha(2)\phi_a\alpha(3)) \\ & + \phi_c\alpha(1)(\phi_a\alpha(2)\phi_b\beta(3) - \phi_b\beta(2)\phi_a\alpha(3)) \end{aligned} \quad (1.1)$$

This class of multiple determinant methods is known as multi-configuration (MC) or multi-reference (MR) methods, where multiple determinants are used in the theoretical method such that electronic states consisting of multiple spin determinants can be rigorously described. Similarly to single reference methods, a self-consistent field (SCF) calculation is needed as the basis for the calculation. Multi-configuration self-consistent field (MCSCF) methods incorporate an iterative method to converge a wave function that has multiple Slater determinants. The choice of which determinants to include in the wave function is a balance between few enough configurations to ensure convergence stability and a large enough number of configurations to adequately describe the system. A popular choice for the determinants to include in a multi-configuration wave function is the complete active space method (CAS), where a

number of active orbitals and active electrons are each specified.¹² Assuming the electrons are counted back from the HOMO, this completely defines which orbitals are involved in the active space. The method states that any possible configuration that can be formed within just these active orbitals and active electrons is included in the wave function. The number of determinants can be seen to increase rapidly with the number of active orbitals, so careful choice of the active space is key.¹³ The electron correlation not included in the MCSCF is referred to as dynamic electron correlation. Due to the lack of dynamic electron correlation, the energies of MCSCF wave functions are not typically used, but are desired as a reference to further post SCF calculations. However, MCSCF wavefunctions can be biased towards certain desired states during their SCF procedures, which will bias any further calculations.^{14,15} Therefore, many MCSCF routines will average the wave functions over all desired states of interest. This produces MCSCF energies that aren't useful as excited state energies without further calculations. This results in a wave function with the proper flexibility with respect to the molecular system, but energies that are not reliable until after post SCF calculations.

An alternative MCSCF method to CASSCF is the general valence bond (GVB) theory, which uses multiple determinants in the wave function to handle wave functions that give correct dissociation curves for molecular systems.¹⁶ GVB wave functions are differing from CASSCF wave functions in that the small number of determinants included are directly specified. The generalized valence bond perfect pairing (GVB-PP) is particularly useful since it is restricted to open shell orbitals and closed shell orbital pairs. Since the SCF algorithm is efficient, the GVB-PP method can be used for geometry optimizations for modestly large systems.¹⁶ Similar to other MCSCF wave

functions, it includes no dynamic correlation and relies on post SCF methods to include dynamic correlation in the final energy. The lightweight wave function makes GVB method a popular choice for reference wave functions for large systems.

Analogous to HF calculations, additions to the multi-configuration wave function are needed to account for dynamic correlation in order to obtain energies that match experiment. The two approaches used to account for dynamic correlation are configuration interaction (CI) and perturbation theory (PT). CI expands a given wave function to a certain number of excitations without changing the wave function orbital coefficients according to an energy minimization equation, and solves for the expansion coefficients to obtain a new wave function.¹⁷ Expanding this methodology to multiple determinants in a multi-configuration wave function results in a multi-reference configuration interaction (MRCI) calculation. While a full CI solves for all possible excitations, the scope of these calculations is only tractable for small molecular systems. Instead, only a subset of excitations are included.¹⁷ When properly applied to a given system, these calculations result in good energies and excited state orbitals to analyze since it produces a new wave function.¹⁷ However, due to only allowing certain excitations within a CI expansion, this method runs into the issues of size inconsistency.¹⁸ Size inconsistent methods are such that the energy of two molecular systems at infinite distance does not equal the sum of the two systems independently.¹⁸ This leads to the method not being reliable for system where the substrate is analyzed as a function of distance from the catalyst.

The other main multi-configuration addition to a MCSCF wave function is to add a perturbation to the energy expression. Many methods are available that add different

perturbations to the MCSCF wave function, NEVPT2 being one of the more recent and popular methods.¹⁹⁻²¹ While each method can have its own stability challenges, they can provide very reasonable energies for each excited state. However, PT approaches only improve the energy of the system, not the wave function itself. Any orbital analysis is performed on the MCSCF wave function, which may not be the best representation of the state of interest. Any multi-configuration approach also suffers from the problem of the required computational resources needed. For all but the smallest organic molecules, geometry optimizations are infeasible. Therefore, any geometry including excited state distortions must be calculated with a different approach.

Due to the complications and computing resources needed for multi-configuration methods, many researchers turn towards DFT to study transition metal complexes. The reasoning behind this choice is obvious. DFT is not significantly slower than HF calculations, but produces improved energies and geometries that match experimental results very well. In addition, time-dependent density functional theory (TDDFT) can describe single excitations better than the HF equivalent methods. The key is that density functional provides electron correlation through the functional's form, and the variety of available functionals allows the functionals themselves to be tuned to work the best for certain molecular systems. In addition, all modern chemistry software packages implement DFT in the form similar to Hartree-Fock such that the implementation algorithms have become highly efficient due to advances in single Hamiltonian SCF accelerators.²² Many packages have analytical first and second derivatives for DFT and TDDFT as well as GPU support for integral calculations (the most time intensive portion

of any SCF routine) such that optimizing ground and TDDFT excited state structures can be accomplished by anyone with a modern workstation.

For these systems, the major hurdle with DFT excited state calculations is that DFT is a single determinant method, making it incompatible with many important excited states. Unlike HF where one can add additional wave function contributions in a CI expansion, a CI expansion of a DFT wave function results in double counting of electron correlation contributions. The DFT functional already includes static and dynamic correlation, so the addition of CI excitations adds correlation that has already been added to the wave function. This is the heart of the “double counting problem” for multi-reference DFT. Many different strategies have been proposed to implement a DFT form that obtains better excited states for non-single determinant electronic configurations while avoiding any double counting issues.

The earliest strategies revolve around broken symmetry approximations. Broken symmetry refers to breaking the symmetry of the alpha and beta electrons by allowing the electrons to occupy potentially different orbitals. For example, a spin-restricted singlet O₂ calculation would put both electrons in one of the π^* orbitals. However, a lower energy configuration is found by allowing each electron in the HOMO to occupy one π^* orbital. The unrestricted representation breaks the symmetry between the alpha and beta wave functions. This alone does not fix the issue in that the broken symmetry wave function is still not a multi-determinant representation, but several methods have used this broken symmetry wave function to provide an approach that mimics a multi-determinant wave function.

Many different approaches have been suggested to obtain better energies from broken symmetry calculations. All of these approaches are looking for solution to the equation for the coupling energy between determinants represented by the Heisenberg Hamiltonian

$$H_{\text{coupling}} = -2J_{ab} \mathbf{S}_a \cdot \mathbf{S}_b \quad (1.2)$$

where \mathbf{S}_a and \mathbf{S}_b are the total spin operators for the two spin states and J_{ab} is the effective exchange integral between the determinants averaged over all orbitals.^{23,24}

The form of J_{ab} has been treated as mostly empirical, and several different forms of J_{ab} have been suggested. The most popular J_{ab} form that was developed to obtain better energies from broken symmetry calculations is the Noodleman projection, which has the form

$$J_{ab} = -\frac{(E_{HS} - E_{BS})}{S_{\text{max}}^2} \quad (1.3)$$

where E_{HS} and E_{BS} are the energies of the high spin and broken symmetry DFT calculations respectively and S_{max}^2 is the total spin for the state with the highest spin.²³

Another popular form of J_{ab} is the Soda projection where J_{ab} is defined as

$$J_{ab} = -\frac{(E_{HS} - E_{BS})}{\langle S^2 \rangle_{HS} - \langle S^2 \rangle_{BS}} \quad (1.4)$$

where $\langle S^2 \rangle_{HS}$ and $\langle S^2 \rangle_{BS}$ the total spin angular momentum for the high spin and broken symmetry calculations.²⁴ A further discussion of broken symmetry methods is included in Appendix A.

All of these broken symmetry projection methods do improve the excitation energies obtained compared to the broken symmetry calculations, but a general

consensus on which form of J_{ab} is the best for all cases is not available. The only benchmarks comparing all methods have been limited to small cases where full-CI calculations are feasible.²⁴ These broken symmetry methods also rely on the converged SCF states for the high-spin and broken-symmetry calculations to be suitable for the J_{ab} approximations. While these methods are convenient to apply to many systems, more rigorous methods that converge multiple determinants simultaneously are more desirable.

Rather than improvements to only the energy, several proposed theories have been suggested to bring multi-configuration character to DFT. The primary obstacle is handling the double counting problem without large alterations to the functionals themselves. The double counting problem is centered around how different methods add different types of correlation to their calculations. Multi-configuration wave functions add static correlation to a wave function while CI and PT methods add dynamic correlation. DFT correlation functionals contain static and dynamic correlation, which is not separable.²⁵ Thus, adding DFT correlations to each wave function in a MC wave function would be double counting correlation effects, causing additional errors in the energy expression.

The earliest attempt at MC DFT approach rely on a modified form of CASSCF that is compatible with DFT by Leininger et al. and Miehlich et al.^{26,27} These methods rely on a partition of DFT correlation contributions to ensure the wave function does not collapse back to a single determinant.²⁶⁻²⁹ These methods do show an improvement over standard DFT calculations and are comparable to CI methods for atoms and

diatomic systems, but can still suffer from double counting errors of static correlation originating from two separate sources.^{28,29}

An ensemble reference approach has been suggested as a way of introducing DFT correlation into highly correlated systems. The most popular version of this ensemble approach is the spin-restricted, ensemble-referenced (REKS) DFT method.³⁰ Using a combination of differences between multiple single determinant DFT wave functions, they arrive at a wave function that incorporates effective differences between certain spin states for two coupled orbitals.³⁰ This method has been expanded to four coupled orbitals and linked to GVB-PP formalism.^{31,32} This method is successful in improving energies for highly correlated systems, but is only rigorously defined for two and four orbitals and only for coupled closed shell orbitals, not singly occupied orbitals.

Recent MCDFT approaches have employed the idea of using only HF exchange terms so that inter-determinant exchange is handled analogously to post-HF methods. The density-functional-based valence bond (DFVB) method by Ying et al. uses a valence bond wave function combined with DFT correlation functionals.²⁵ The idea behind this combination is that VB wave functions have no dynamic correlation, so the use of DFT correlation functionals can provide an inexpensive means to providing dynamic correlation compared to PT or CI approaches without significant double counting.²⁵ However, analogous to PT and CI methods, the DFT correlation is added onto a fixed VB wave function. While the density used to calculate the correlation is allowed to change until self-consistency, the VB coulomb and exchange contributions do not.

Similar approaches to DFVB have been tried using other MCSCF wave functions as the reference.³³ A recent approach has been detailed Manni et al. where a CASSCF wave function is used with a DFT correlation functional applied on top non-self consistently to form the multiconfiguration pair-density functional theory (MC-PDFT).³⁴ While the authors used improvements to the DFT functionals by forming pair-density functionals from traditional popular functions, the correlation is not treated with a SCF approach.³⁴ This is different from traditional DFT methods (by which DFT functionals are benchmarked and tuned) where coulomb, HF exchange, and DFT exchange/correlation contributions are converged simultaneously. These methods do lead to an improvement over their counterparts without the DFT correlation, but still have significant errors with respect to excitation energies for O and O₂.

SPECIFIC AIMS OF THIS RESEARCH:

In chapter II, I will describe a new DFT method named few determinant density functional theory (FD-DFT) meant to overcome the double counting issue while providing multi-determinant character to DFT calculations. As the name suggests, the method focuses on including only the determinants needed to provide static correlation to the calculation while leaving out any determinants that contribute to local dynamic correlation already included in the correlation functional. The concepts introduced in this chapter describe a generic form for combining multiple determinants coherently, and will be implemented in terms of excited state multiplets using a general valence bond (GVB) theory framework. The method is applied to benchmark cases to show its utility.

In chapter III, the excited states of a Cr(III)(AcAc)₃ analog are calculated using a MRCI based method named spectroscopy oriented configuration interaction (SORCI) as

well as FD-DFT. Cr(III)(AcAc)₃ systems have been long studied as they exhibit unique properties in their excited states, such as intersystem crossing (ISC) rates that exceed vibrational cooling rates. This system is analyzed in detail to understand the fast intersystem crossing rate and benchmark the viability of this method for understanding other first-row transition metal complexes in terms of their excited states.

In chapter IV, the quenching of Cr(III) catalysts by O₂ is studied in order to understand the mechanism of this quenching event. Using single determinant DFT, FD-DFT, and CASSCF with NEVPT2, the excited states of this system are explored to find the excited state by which this quenching event occurs. The importance of using methods with multi-determinant properties is highlighted by comparison with standard DFT calculations by analyzing the excited states through the spin-density plots of each excited state.

Chapter V focuses on a comprehensive theoretical study of chromium and vanadium complexes to demonstrate the large differences between isoelectronic chromium and vanadium complexes with identical ligand structures. Using TDDFT excitation spectra, spin density plots, vibrational component plots of excited state distortions, and SORCI excited state potential energy curve plots, the surprising differences between these chromium and vanadium complexes are explored. The theoretical results agree with experimental observations related to vanadium complex reactivity, highlighting the importance of metal center choice in transition metal photocatalyst design.

REFERENCES

- (1) Cano-Yelo, H.; Deronzier, A. *Tetrahedron Lett.* **1984**, 25 (48), 5517–5520.
- (2) Meyer, T. J. *Acc. Chem. Res.* **1989**, 22 (5), 163–170.
- (3) Yoon, T. P.; Ischay, M. A.; Du, J. *Nat. Chem.* **2010**, 2 (7), 527–532.
- (4) Narayanam, J. M. R.; Stephenson, C. R. J. *Chem Soc Rev* **2011**, 40 (1), 102–113.
- (5) Tucker, J. W.; Stephenson, C. R. J. *J. Org. Chem.* **2012**, 77 (4), 1617–1622.
- (6) Xuan, J.; Xiao, W.-J. *Angew. Chem. Int. Ed.* **2012**, 51 (28), 6828–6838.
- (7) Prier, C. K.; Rankic, D. A.; MacMillan, D. W. C. *Chem. Rev.* **2013**, 113 (7), 5322–5363.
- (8) Gordon B. Haxel; Sara Boore; Susan Mayfield. U.S. Geological Survey November 20, 2002.
- (9) Stevenson, S. M.; Shores, M. P.; Ferreira, E. M. *Angew. Chem. Int. Ed.* **2015**, 54 (22), 6506–6510.
- (10) Higgins, R. F.; Fatur, S. M.; Shepard, S. G.; Stevenson, S. M.; Boston, D. J.; Ferreira, E. M.; Damrauer, N. H.; Rappé, A. K.; Shores, M. P. *J. Am. Chem. Soc.* **2016**, 138 (16), 5451–5464.
- (11) Ashley, D. C.; Jakubikova, E. *Coord. Chem. Rev.* **2017**, 337, 97–111.
- (12) Roos, B. O.; Taylor, P. R.; Si \equiv gbahn, P. E. M. *Chem. Phys.* **1980**, 48 (2), 157–173.
- (13) Szalay, P. G.; Müller, T.; Gidofalvi, G.; Lischka, H.; Shepard, R. *Chem. Rev.* **2012**, 112 (1), 108–181.
- (14) Ruedenberg, K.; Cheung, L. M.; Elbert, S. T. *Int. J. Quantum Chem.* **1979**, 16 (5), 1069–1101.

- (15) Barbatti, M.; Shepard, R.; Lischka, H. In *Conical Intersections: Theory, Computation and Experiment*; World Scientific, 2011.
- (16) Bobrowicz, F. W.; William A. Goddard Iii. In *Methods of Electronic Structure Theory*; III, H. F. S., Ed.; Modern Theoretical Chemistry; Springer US, 1977; pp 79–127.
- (17) Jensen, F. *Introduction to computational chemistry*, 2nd ed.; John Wiley & Sons: Chichester, England; Hoboken, NJ, 2007.
- (18) Pople, J. A.; Binkley, J. S.; Seeger, R. *Int. J. Quantum Chem.* **1976**, *10* (S10), 1–19.
- (19) Angeli, C.; Cimiraglia, R.; Evangelisti, S.; Leininger, T.; Malrieu, J.-P. *J. Chem. Phys.* **2001**, *114* (23), 10252–10264.
- (20) Angeli, C.; Cimiraglia, R.; Malrieu, J.-P. *J. Chem. Phys.* **2002**, *117* (20), 9138–9153.
- (21) Angeli, C.; Pastore, M.; Cimiraglia, R. *Theor. Chem. Acc.* **2007**, *117* (5–6), 743–754.
- (22) Pulay, P. *J. Comput. Chem.* **1982**, *3* (4), 556–560.
- (23) Noodleman, L.; Davidson, E. R. *Chem. Phys.* **1986**, *109* (1), 131–143.
- (24) Soda, T.; Kitagawa, Y.; Onishi, T.; Takano, Y.; Shigeta, Y.; Nagao, H.; Yoshioka, Y.; Yamaguchi, K. *Chem. Phys. Lett.* **2000**, *319* (3), 223–230.
- (25) Ying, F.; Su, P.; Chen, Z.; Shaik, S.; Wu, W. *J. Chem. Theory Comput.* **2012**, *8* (5), 1608–1615.
- (26) Leininger, T.; Stoll, H.; Werner, H.-J.; Savin, A. *Chem. Phys. Lett.* **1997**, *275* (3), 151–160.

- (27) Miehllich, B.; Stoll, H.; Savin, A. *Mol. Phys.* **1997**, *91* (3), 527–536.
- (28) Ukai, T.; Nakata, K.; Yamanaka, S.; Takada, T.; Yamaguchi, K. *Mol. Phys.* **2007**, *105* (19–22), 2667–2679.
- (29) Kurzweil, Y.; Lawler, K. V.; Head-Gordon, M. *Mol. Phys.* **2009**, *107* (20), 2103–2110.
- (30) Filatov, M.; Shaik, S. *J. Phys. Chem. A* **2000**, *104* (28), 6628–6636.
- (31) Filatov, M.; Liu, F.; Kim, K. S.; Martínez, T. J. *J. Chem. Phys.* **2016**, *145* (24), 244104.
- (32) Filatov, M.; Martínez, T. J.; Kim, K. S. *Phys Chem Chem Phys* **2016**, *18* (31), 21040–21050.
- (33) Ángel J. Pérez-Jiménez; José M. Pérez-Jordá; Juan C. Sancho-García. *J. Chem. Phys.* **2007**, *127* (10), 104102.
- (34) Manni, G. L.; Carlson, R. K.; Luo, S.; Ma, D.; Olsen, J.; Truhlar, D. G.; Gagliardi, L. *J. Chem. Theory Comput.* **2014**, *10* (9), 3669–3680.

CHAPTER 2: FEW-DETERMINANT DENSITY FUNCTIONAL THEORY (FD-DFT), SPIN MULTIPLETS AS PROOF OF CONCEPT

INTRODUCTION:

From molecular oxygen to classical coordination complexes, compounds with a set of degenerate or nearly degenerate partially filled orbitals provide unique radical stability as well as unique electronic spectroscopy due to low lying excited states of reduced spin multiplicity. Theoretical calculations of these systems is complicated by the need for multiple determinants to adequately describe these states.

Systems where a set of n electrons are described by n intrinsically orthogonal orbitals have degenerate ground states where the ground state degeneracy can be split by a magnetic field into $n+1$ states. This degenerate set of states is referred to as a spin multiplet. Examples of spin multiplets include most atomic systems such as 3P oxygen atom, molecular systems such as $^3\Sigma$ O₂ and 3B_1 methylene, and an abundance of first-row transition metal coordination complexes. Spin recoupling amongst multiplet electrons leads to low lying excited states. While the $M_s = S_{\max}$ ground multiplet state can be described by a single Slater determinant, the lower M_s microstates as well as the low-lying electronic excited states require more than one determinant. The multi-determinant nature of multiplet states, as well as the challenges posed to density functional theory have been long recognized.¹⁻⁸

For example for O₂, while the $M_s = \pm 1$ components of the ground state triplet multiplet can be described by a single determinant, the $M_s = 0$ component of the ground state as well as each of the excited state configurations require two determinants. As

recognized in 1977, this poses a challenge for single determinant density functional models.⁹ Within DFT, the $\pi_x^*, \pi_y^* \alpha\alpha$ ground state, a $\pi_x^*, \pi_y^* \alpha\beta$ broken symmetry wave function (described in Appendix A), and a $\pi_x^*, \pi_x^* \alpha\beta$ configuration can be computed. The broken symmetry solution underestimates the energy of the $^1\Delta$ state by 0.5 eV. Estimates for the $^1\Delta$ state can be provided by a sum rules model⁹. Electron correlation amongst the multiplet set of electrons is well described by a Hartree-Fock wave function. The Pauli Principle dictated wave function antisymmetry correlates electrons of the same spin.

Ranging from the multiplet structure of open shell transition metal coordination complexes to the dissociation of chemical bonds, there are a number of important problems that are intrinsically multi-determinant, yet pragmatically require the dynamic correlation easily described by density functional theory (DFT). Here we sketch a few-determinant density functional theory approach (FD-DFT) that has been developed and applied to magnetic interactions¹⁰ as well as low lying excited states of coordination complexes.¹¹ The current approach builds off the sum rules approach from the 1970s⁹ as well as the more recent spin-flip approaches.^{12,13} By reformulating the problem as a linear combination of a small number of Slater determinants a variational treatment of the wave function/density can be achieved for multiplet systems.

THEORY:

FD-DFT THEORY:

In the FD-DFT approach described here inter-determinant coupling terms are evaluated using a finite difference approach. As has been long recognized, incorporation of a spin restricted exchange-correlation term is an unmet challenge.¹⁴ At

least two determinants are needed and the non-separability of density functional exchange is an issue, see for example the work by Pérez-Jiménez et al.¹⁵ In Hartree Fock the total exchange energy, E_x , is a pairwise sum of individual exchange integrals, whereas in DFT the total exchange energy cannot be separated into individual terms.

The Restricted Open shell Kohn Sham (ROKS) approach of Russo, Martin, and Hay¹⁶ provides a hint as to how to proceed. In the ROKS model a density functional exchange-correlation term is variationally incorporated into an open shell spin restricted model by computing α and β exchange-correlation potential matrices forming linear combinations and adding them to the α and β Fock matrices. For example, for a system of n closed shell electrons and $n_\alpha - n_\beta$ open shell electrons Eq. (2.1) and (2.2) result.

$$\mathbf{F}_\alpha = \mathbf{h}^{core} + \sum_{j=1}^{n_\beta} (2\mathbf{J}_j - \mathbf{K}_j) + \sum_{j=n_\beta+1}^{n_\alpha} (\mathbf{J}_j - \mathbf{K}_j) + \mathbf{V}_\alpha^{xc} \quad (2.1)$$

$$\mathbf{F}_\beta = \mathbf{h}^{core} + \sum_{j=1}^{n_\beta} (2\mathbf{J}_j - \mathbf{K}_j) + \sum_{j=n_\beta+1}^{n_\alpha} \mathbf{J}_j + \mathbf{V}_\beta^{xc}$$

$$\mathbf{F}_C = \frac{\mathbf{F}_\alpha + \mathbf{F}_\beta}{2} = \mathbf{h}^{core} + \sum_{j=1}^{n_\beta} (2\mathbf{J}_j - \mathbf{K}_j) + \frac{1}{2} \sum_{j=n_\beta+1}^{n_\alpha} (\mathbf{J}_j - \mathbf{K}_j) + \sum_{j=n_\beta+1}^{n_\alpha} \mathbf{J}_j + \frac{1}{2} (\mathbf{V}_\alpha^{xc} + \mathbf{V}_\beta^{xc}) \quad (2.2)$$

$$\mathbf{F}_O = \mathbf{F}_\alpha + \mathbf{V}_\alpha^{xc}$$

In order to see how to proceed to the general multiplet system, consider a system of two electrons and two orthogonal orbitals (ϕ_a and ϕ_b). Single determinant $M_s = 0$ and $M_s = 1$ wave functions are given in Eq. (2.3) and (2.4).

$$\Psi_{M_s=0} = \phi_b \phi_a \alpha \beta \quad (2.3)$$

$$\Psi_{M_s=1} = \phi_b \phi_a \alpha \alpha \quad (2.4)$$

The $M_s = 0$ single determinant Hartree Fock energy is given in Eq. (2.5) and the $M_s = 1$ single determinant Hartree Fock energy in Eq. (2.6).

$$E_{M_S=0} = h_{aa} + h_{bb} + J_{ab} \quad (2.5)$$

$$E_{M_S=1} = h_{aa} + h_{bb} + J_{ab} - K_{ab} \quad (2.6)$$

The sum rules singlet energy of Ziegler, Rauk, and Baerends is given in Eq. (2.7)

$$E_{\text{singlet}} = 2E_{M_S=0} - E_{M_S=1} \quad (2.7)$$

where substitution of Eq. (2.5) and (2.6) into Eq. (2.7), yields the correct open-shell singlet Hartree-Fock energy, Eq. (2.8).⁹

$$E_{\text{Singlet}} = h_{aa} + h_{bb} + J_{ab} + K_{ab} \quad (2.8)$$

An alternative development is to take the open-shell singlet wave function as a linear combination of the two $M_s = 0$ determinants, Eq. (2.9).

$$\Psi_{\text{Singlet}} = \Psi_{\alpha\beta} + \Psi_{\beta\alpha} \quad (2.9)$$

$$E_{\text{Singlet}} = \frac{1}{2} (E_{\alpha\beta} + E_{\beta\alpha} - 2H_{\text{coupling}}) \quad (2.10)$$

$$E_{\alpha\beta} = E_{\beta\alpha} = h_{aa} + h_{bb} + J_{ab} \quad (2.11)$$

$$H_{\text{coupling}} = -K_{ab} \quad (2.12)$$

For a Hartree-Fock treatment, the coupling term, K_{ab} , can be obtained, rather than through direct computation, as the difference between the $M_s = 1$, Eq. (2.13), and the $M_s = 0$, Eq. (2.11), single-determinant total electronic energies, see Eq. (2.14).

$$E_{\alpha\alpha} = h_{aa} + h_{bb} + J_{ab} - K_{ab} \quad (2.13)$$

$$H_{\text{coupling}} = E_{\alpha\alpha} - \frac{1}{2} (E_{\alpha\beta} - E_{\beta\alpha}) = -K_{ab} \quad (2.14)$$

In a DFT formulation of the above two determinant model, $E_{\alpha\alpha}$ and $E_{\alpha\beta}$ can be simply replaced by their DFT counterparts. The energy expressions of Eq. (2.11) and (2.13) become Eq. (2.15) - (2.17) where the densities reflect the underlying spin.

$$E_{\alpha\beta} = E_{\beta\alpha} = h_{aa} + h_{bb} + J_{ab} + E^{\text{xc}}(\rho_{\alpha\beta}) \quad (2.15)$$

$$E_{\beta\alpha} = E_{\beta\alpha} = h_{aa} + h_{bb} + J_{ab} + E^{\text{xc}}(\rho_{\beta\alpha}) \quad (2.16)$$

$$E_{\alpha\alpha} = E_{\beta\alpha} = h_{aa} + h_{bb} + J_{ab} + E^{xc}(\rho_{\alpha\alpha}) \quad (2.17)$$

The coupling term analogous to Eq. (2.14) is given by Eq. (2.18).

$$H_{\text{coupling}} = E_{\alpha\alpha} - \frac{1}{2}(E_{\alpha\beta} + E_{\beta\alpha}) = E^{xc}(\rho_{\alpha\alpha}) - \frac{1}{2}(E^{xc}(\rho_{\alpha\beta}) + E^{xc}(\rho_{\beta\alpha})) \quad (2.18)$$

Exchange coupling terms for the general case can be obtained from determinants that are two spin flips removed from high spin determinant. This allows for a linearly independent solution for each of the approximate DFT exchange-correlation energy terms using the expression

$$K_{ij}^{xc} = \sum_{m,n}^{n_o} c_{mn}^{ij} (E_{HS}^{xc}[\rho_{HS}] - E_{mn}^{xc}[\rho_{mn}]) \quad (2.19)$$

where n_o is the number of open shell electrons, m and n are the electrons flipped relative to the high spin determinant, c_{mn}^{ij} is the coefficient needed for the spin flipped determinant to obtain the exchange-correlation energy for electrons i and j , E_{mn}^{xc} is the DFT exchange-correlation energy for the high spin determinant, E_{mn}^{xc} is the DFT exchange-correlation energy for the double spin flipped determinant, and K_{ij}^{xc} is the DFT exchange-correlation energy between electrons i and j . In addition to the already described two-electron special case other exception to this general method is the four open shell electron system due to the existence of only three unique double spin flip determinants, this system requires an alternative procedure to obtain the exchange-correlation energies (see Appendix B).

In addition to being useful for spin restricted open shell systems, the approach can be used for a more general set of wave functions. The total energy for any electronic wave function can be described in terms of one and two-electron density matrices, D_i and D_{ij} respectively Eq. (2.20).

$$E = \sum_{i,j}^n D_j^i h_{ij} + \sum_{i,j}^n D_{kl}^{ij} (ij | kl) \quad (2.20)$$

If the density matrices are reduced to diagonal form the general perfect-pair and multiplet energy expression and Fock matrices are given by Eq. (2.21)

$$E = 2 \sum_i f_i h_{ii} + \sum_i \sum_j (a_{ij} J_{ij} + b_{ij} K_{ij}) \quad (2.21)$$

$$E = \sum_i f_i h_{ii} + \langle \phi_i | F_i | \phi_i \rangle$$

In the general energy expression, f_i are the occupation numbers (diagonal one-electron density matrix elements) for the individual orbitals. For doubly-occupied orbitals f_i is 1. For singly-occupied orbitals f_i is $\frac{1}{2}$ and for paired orbitals f_i is the CI coefficient c_i^2 . The a_{ij} and b_{ij} coefficients are derived either from the intrinsic multiplet structure of the wave function or from variational pair-wise CI coefficients.

In density functional theory, the corresponding electronic energy expression can be written as

$$E = 2 \sum_i f_i h_{ii} + \sum_i \sum_j (a_{ij} J_{ij} + b_{ij} K_{ij}^*) \quad (2.22)$$

where the exchange energy, K_{ij}^* is a combination of exact exchange and DFT exchange terms

$$K_{ij}^* = AK_{ij} + (1-A)K_{ij}^{xc} \quad (2.23)$$

As described in Eq. (2.19) the DFT exchange energy, K_{ij}^{xc} can be described by a linear combination of determinant-based exchange energies.

The variational exchange operator, \mathbf{K}_j^* can be described as a combination of exact exchange and DFT exchange operators

$$\mathbf{K}_j^* = A\mathbf{K}_j + (1-A)\mathbf{V}_j^{xc} \quad (2.24)$$

where the DFT exchange operator, \mathbf{V}_j^{xc} consists of linear combinations of exchange correlation potentials

$$\mathbf{V}_j^{xc} = \sum_m c_m^j V_j^{xc} [\rho_m] \quad (2.25)$$

Non-separability leads to the DFT exchange energy, K_j^{xc} not being equal to the sum of DFT exchange operators

$$K_j^{xc} \neq \sum_j \langle \phi_i | c_m V_j^{xc} [\rho_m] | \phi_i \rangle \quad (2.26)$$

The derivative of Eq. (2.25) with respect to ρ_α or ρ_β yields Fock matrix expressions in terms of conventional density functional exchange-correlation potentials. Like the exchange energies obtained from DFT determinants, exchange-correlation potentials between the determinants are needed. However, the presence of separate α and β potentials simplifies separating the potential between determinants. The high spin determinant potential can be expressed as

$$\begin{aligned} V_{HS,\alpha}^{xc} &= V_C^{xc} + \sum_{i=1}^n \sum_{j=1}^n V_{i(j)}^{xc} \\ V_{HS,\beta}^{xc} &= V_C^{xc} \end{aligned} \quad (2.27)$$

where $\mathbf{V}_{HS,x}^{xc}$ is the total α / β potential for the high spin determinant, \mathbf{V}_C^{xc} is the potential for all closed shell electrons as well as the open shell electrons with the core electrons, and $\mathbf{V}_{i(j)}^{xc}$ is the potential for open shell electron i on open shell electron j . Each single spin flip potential can be expressed as

$$\begin{aligned} \mathbf{V}_{l,\alpha}^{xc} &= \mathbf{V}_C^{xc} + \sum_{i \neq l}^n \sum_{j=1}^n \mathbf{V}_{i(j)}^{xc} \\ \mathbf{V}_{l,\beta}^{xc} &= \mathbf{V}_C^{xc} + \sum_{j=1}^n \mathbf{V}_{l(j)}^{xc} \end{aligned} \quad (2.28)$$

where l is the electron that has been flipped to β .

While the closed shell potential is trivial to obtain, there are two alternative ways to separate the individual open shell potentials. Subtracting the high spin α potentials from the spin flipped α potential yields the DFT potential for only the single spin flipped electron. Using the β potentials yields the same potential plus a sign change

$$\begin{aligned} \mathbf{V}_{HS,\beta}^{xc} &= \mathbf{V}_C^{xc} \\ \mathbf{V}_{HS,\alpha}^{xc} - \mathbf{V}_{I,\alpha}^{xc} &= \sum_{j=1}^n \mathbf{V}_{I(j)}^{xc} \\ \mathbf{V}_{I,\beta}^{xc} - \mathbf{V}_{HS,\beta}^{xc} &= \sum_{j=1}^n \mathbf{V}_{I(j)}^{xc} \end{aligned} \quad (2.29)$$

The energy and potential expressions in Eq. (2.19) and (2.29) can be used to replace the HF exchange terms in any method that can be described with diagonal two-electron density matrices.

GVB IMPLEMENTATION:

The FD-DFT equations for the energy and potential terms are independent from the method used to obtain the total energy. We have chosen to implement the FD-DFT method within a generalized valence bond (GVB) formalism. Specifically, the perfect pairing (GVB-PP) theory was used as the foundation for the SCF routines due to some advantageous properties of the GVB-PP model. First, using the PP simplifications to the GVB wave function, the computational effort is less than doubled relative to a ROHF wave function implemented through a single effective Hamiltonian. Second, in our initial testing, we found a GVB implementation of the FD-DFT scheme more stable for a variety of test cases over a single effective Hamiltonian implementation using a direct inversion in the iterative subspace (DIIS) optimizer.

The additions to a GVB-PP wave function implementation are straightforward. The GVB formalism used in this implementation is detailed by Bobrowicz and

Goddard.¹⁷ The GVB wave function is constructed to consist of $n_o + 1$ individual Hamiltonians where the closed shell (doubly occupied) orbitals occupy the first Hamiltonian and each open shell orbital is put into a separate Hamiltonian. Since the FD-DFT formalism is only defined for multiplets in this work, each open shell orbital contains one electron.

The GVB algorithm is the same as the standard implementations using HF Hamiltonians except for the following additions: calculation of the DFT energies and potentials for each determinant, calculating the inter-determinant exchange energies, calculating the DFT potentials for each open shell orbital, performing the DFT multiplets CI, calculating the a_{ij} and b_{ij} scalars (diagonal two-electron density matrix elements) for the desired excited state, calculating the total energy, and performing the orbital mixing with the DFT open shell potentials. The calculation of the individual DFT determinant energies and potentials is performed after the calculation of the HF potentials. For any number of open shell electrons, the high spin determinant, all single spin flip determinants, and all double spin flip determinants are calculated using standard DFT routines, which gives a single energy and α/β potentials for each determinant. The determinants calculated are independent of the desired excited state. The approximate inter-determinant exchange energies are calculated according to Eq. (2.19) by matrix inversion. The DFT potentials are calculated according to (2.29). The “ α ” form of the open shell potentials was chosen for convenience.

Having obtained approximations for all the energies needed to construct any multiplet, all that is needed is to construct the desired state. A small CI scheme that involves only the possible spin multiplet combinations without any paired open shell

orbitals and no excitations out of the open shell space is used to calculate eigenstates of a spin Hamiltonian. The basis set for the Hamiltonian consists of only all possible spin flips of the open shell electrons of the high spin determinant. The diagonal elements consists of closed shell energy (both Hartree-Fock coulomb and fractional exchange as well as DFT exchange-correlation) plus any exchange-correlation energies between open shell electrons (HF and DFT) in that state. Any off-diagonal Hamiltonian elements in the CI consist of allowed exchange terms that are equal to proper HF and DFT exchange-correlation energies. All other elements are zero.

The resulting Hamiltonian is small, so is directly diagonalized. This directly yields the energies and eigenvectors for all possible multiplet states. Selecting the desired state from the CI yields the eigenvector that determines the combination of determinants needed to recover the DFT energy in subsequent iterations of an SCF iteration scheme. The determinant combination provides the DFT portion of the energy expressions. This is transformed to the b_{ij} values by accounting for all valid exchanges within the determinant and between individual determinants. All a_{ij} values are set to 1.

The total energy is calculated according to Eq. (2.22) with care to remove any DFT energy contributions from the DFT potentials due to the consequences of Eq. (2.26). The DFT Fock matrices are used to obtain variational mixing between occupied and virtual orbitals using OCBSE and between occupied orbitals of different shells using rotational mixing, the rotation coefficient given in Eq. (2.30)

$$\lambda = -\frac{\mathbf{B}_{0,ij}}{\mathbf{B}_{ij,ij}} \quad (2.30)$$

where $B_{0,ij}$ is given in Eq. (2.31) and $B_{ij,ij}$ estimated by Eq. (2.32)¹⁷

$$B_{0,ij} = \langle i_0 | F_{j_0} | j_0 \rangle - \langle i_0 | F_{i_0} | j_0 \rangle \quad (2.31)$$

$$B_{ij,ij} = [\langle i_0 | F_{j_0} | i_0 \rangle - \langle i_0 | F_{i_0} | i_0 \rangle - \langle j_0 | F_{j_0} | j_0 \rangle + \langle j_0 | F_{i_0} | j_0 \rangle] \quad (2.32)$$

However, Eq. (2.32) in the formal GVB-PP formalism contains an extra parameter, γ_{ij}^{ij} .

The integrals that constitute this parameter have not yet been developed for DFT as they are not combinations of coulomb and exchange integrals, so it is not included, at this time.

APPLICATIONS:

THEORETICAL BENCHMARKING:

In order to test the validity of this approximation to the interdeterminantal exchange energies and potentials for DFT methods, several benchmark cases were studied. All calculations were performed using the cc-pVDZ basis set with HF and DFT for a variety of functionals chosen to represent commonly utilized methods in the literature. The GVB method was chosen for the implementation of the FD-DFT approach while unrestricted calculations utilizing a DIIS optimizer were used for the broken symmetry energies. All excitation energies were obtained from finite differences of the ground and desired excited state. The unrestricted calculations were performed using a standard, unmodified SCF routine. The FD-DFT algorithm was implemented in a modified GVB module within Gaussian. All calculations were performed using the Gaussian 16 suite of electronic structure programs.¹⁸

ATOMIC AND MOLECULAR OXYGEN:

The magnetic field exposed multiplet structure of oxygen atom led Mulliken to an electronic structure description of the $^3\Sigma$ ground state of O_2 as well the observed $^1\Sigma$ excited state.¹⁹ In analogy to the 3P , 1D (1.96 eV), and 1S states (4.18 eV) of O ,²⁰ Mulliken proposed a doubly degenerate excited state for O_2 intermediate in energy

between the observed excitation that he ascribed as being from the $^3\Sigma$ state to the $^1\Sigma$ state.¹⁹ This predicted $^1\Delta$ excited state was subsequently observed providing foundational support for molecular orbital theory.

In addition to being foundational to our understanding of electronic wave functions O_2 is an active participant in photoconversion processes. The triplet nature of ground state O_2 leads to competitive quenching of photoactive excited states²¹ as well as contributing to electronic barriers in the final O_2 dissociation step in the oxygen evolution reaction of water splitting.²²

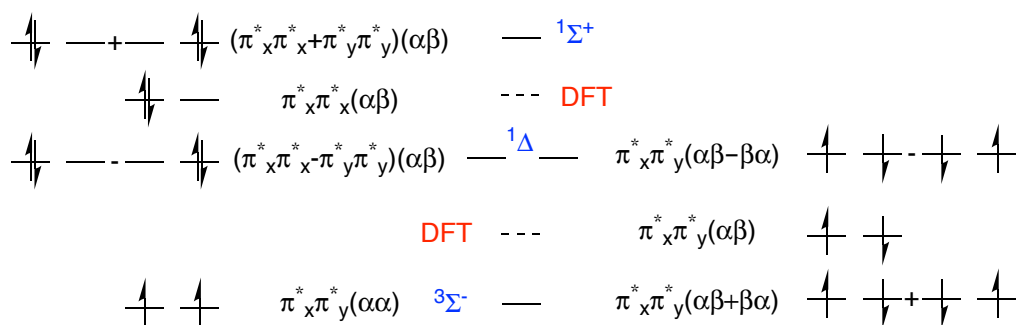


Figure 2.1: Electronic configuration for O_2 ground and excited states. The term symbols for each true state are given in blue while the single determinant states are labeled with the red DFT notation. The spin and spatial orbitals are given for each state as well as an identical arrow style representation.

Despite the long history associated with our understanding of the O_2 electronic wave functions, challenges remain. There are four electronic configurations for two electrons in two orthogonal π^* orbitals. The electronic configuration diagram for O_2 is given in Figure 2.1. As described by Mulliken, the ground state of O_2 consists of two degenerate singly occupied π^* orbitals that are triplet coupled. This triplet coupling provides three multiplet components ($M_s = -1, 0, +1$). The lowest excited state, the $^1\Delta$ state, is comprised of two degenerate electronic configurations. As described by Moss and Goddard, one component of the $^1\Delta$ state can be described as utilizing the same

singly occupied orbitals as the ground state $^3\Sigma$, the electrons singlet coupled rather than triplet coupled.²³ Triplet coupling in the ground state leads to a favorable exchange interaction while singlet coupling in the excited state leads to a repulsive interaction involving the same exchange term. The second $^1\Delta$ component consists of the negative combination of two electronic configurations wherein alternate π^* orbitals are doubly occupied. The negative sign leads to a favorable exchange interaction. The final state, the $^1\Sigma$ state, is the positive combination of doubly occupied π^* orbitals. The positive sign leads to an unfavorable exchange interaction. This analysis suggests a nearly even spacing between the three low-lying states of O_2 , see Table 2.1 for the experimental excitation energies.

While the $M_s = \pm 1$ components of the ground state triplet multiplet can be described by a single determinant, the $M_s = 0$ component of the ground state as well as each of the excited state configurations require two determinants. As recognized in 1977 this poses a challenge for single determinant density functional models.⁹ The broken symmetry solution underestimates the energy of $^1\Delta$ state by 0.5 eV. The experimental O-O bond distances were used for the $^3\Sigma$ and $^1\Delta$ states while the average of the two was used for the broken symmetry state. Results are collected Table 2.1.

Dating from the Racah parameters of inorganic chemistry, multiplets have provided the best experimental measure of intra-atomic exchange interactions.²⁴⁻²⁶ The inability of DFT to describe the multi-determinantal character of multiplets has left only indirect measures of exchange. This lack of a foundational reference point has hindered

Table 2.1: O and O₂ excitation energies from the triplet (³P/³Σ) state to the singlet (¹D/¹Δ) using GVB based FD-DFT, broken symmetry, and FD-DFT without SCF on the excited state for a variety of DFT functionals. All energies are in eV. For the HF calculations, standard GVB wave functions were employed.

O ³ P → ¹ D	HF	B3LYP	B55LYP	APF-D	BLYP	PBEPBE	PBE1PBE	MN15	Exp ²⁰
FD-DFT (SCF)	2.23	1.51	1.60	1.63	1.37	1.49	1.63	0.99	1.95
FD-DFT (CI)	2.26	1.51	1.55	1.63	1.36	1.52	1.63	1.78	
Broken Symmetry	1.01	0.72	0.75	0.78	0.68	0.73	0.77	0.87	
O ₂ ³ S → ¹ D									Exp ²⁷
FD-DFT (SCF)	1.33	0.84	0.97	0.87	0.75	0.76	0.87	0.58	0.98
FD-DFT (CI)	1.34	0.83	0.94	0.80	0.76	0.77	0.86	0.98	
Broken Symmetry	0.73	0.45	0.53	0.46	0.39	0.39	0.46	0.53	

the study of open-shell transition metal complexes. Future functional development and parameterization studies will benefit from the development of FD-DFT.

The theoretical excitation energies for O and O₂ exhibit some interesting trends. As expected, the broken symmetry excitation energies underestimate the excitation energy by ~1.0 eV for O and ~0.5 eV for O₂ for all DFT functionals tested. By contrast, the FD-DFT energies come much closer to the experimental values. The performance of the FD-DFT method is better for diatomic oxygen rather than atomic oxygen. Interestingly, calculating the excitation energy by CI excitation from the FD-DFT high spin wave function provides a reasonable estimation for the excitation energy without the expense of a SCF procedure on the excited state. The choice of functional also has a large impact on the FD-DFT excitation energy while it has little effect on the broken symmetry excitation energy. The relative amount of exact exchange drastically changes agreement with experimental excitation energies, while functionals containing only DFT exchange terms underestimate the excitation energy by a large amount, although they are still improved over broken symmetry estimations from a hybrid functional.

THREE ELECTRON SYSTEMS, NITROGEN ATOM AND Cr(III) ION:

While the two electron multiplet is the most common example, three to five electron multiplet systems are of interest for earth abundant metal complexes, due to the potential for spin-flipped long-lived excited states. Six-coordinate chromium(III) complexes with a d³ electron configuration possess a ground state ⁴A₂ (octahedral notation) and low lying ²E and ²T₁ excited states which are populated by rapid intersystem crossing from an excited quartet manifold.^{28,29} The doublet excited states possess lifetimes in the microsecond timescale—far longer than substrate diffusion,

making them photochemically relevant.²¹ The ground state 4A_2 as well as the 2E and 2T_1 excited states each place three electrons in the triply degenerate non-bonding t_{2g} orbital set. For a number of Cr(III) complexes these doublet states are simply a set of spin flips from the ground state. As with O_2 the multiplet excited states of Cr(III) require more than one determinant for accurate description.

Progressing from the two active or open shell electrons of oxygen to the three electrons of nitrogen yields four M_s components for the quartet state and now two orthogonal doublet states each with two M_s components. One of the doublets accrues from the two electron triplet spin eigenfunction through addition of a β electron and the other from the two electron open shell singlet spin eigenfunction through the addition of an α electron. For nitrogen the experimental ground state is 4S with 2D and 2P excited states at 2.38 and 3.58 eV.³⁰ For gas phase chromium(III) ion the experimental ground state is a 4F with low lying excited 4P (1.71 eV) and 2G (1.84 eV) excited states.³¹ The 2E and 2T_1 excited states of Cr(III) complexes derive from the 2G atomic state.

Data on the N atom is collected in Table 2.2 and data on the Cr(III) ion is collected in Table 2.3. Results for nitrogen atom show similar trends to the oxygen atom data. As expected the broken symmetry cases underestimate the excitation energy by more than half the experimental value. The FD-DFT excitation energies fall much closer to the experimental excitation energy. DFT functionals with higher percentages of HF exchange give improved energies and pure DFT exchange functionals perform poorly. Interestingly, the MN15 functional, which underestimated the O and O_2 excitation energies the most, had the closest theoretical excitation energies for nitrogen atom. In addition, the two equivalent spin eigenfunctions $2\alpha\alpha\beta - \alpha\beta\alpha - \beta\alpha\alpha$ (2-1-1) and

Table 2.2: Excitation energies for nitrogen atom from the 4S state to the 2D state. Two generate spin eigenfunctions are given for FD-DFT excitation energies (2-1-1 and 1-1). All energies are in eV.

N $^4S \rightarrow ^2D$	HF	B3LYP	B55LYP	APF-D	BLYP	PBEPBE	PBE1PBE	MN15	Exp ³⁰
FD-DFT (SCF) (2-1-1)	2.88	1.81	1.91	2.00	1.67	1.87	1.99	2.42	2.38
FD-DFT (CI) (2-1-1)	2.91	1.79	1.90	1.98	1.61	1.82	1.97	2.42	
FD-DFT (SCF) (1-1)	2.88	1.81	1.91	2.00	1.66	1.86	1.99	2.43	
FD-DFT (CI) (1-1)	2.91	1.79	1.90	1.98	1.61	1.82	1.97	2.42	
Broken Symmetry	1.67	1.11	1.14	1.21	1.01	1.14	1.20	1.60	

Table 2.3: Cr(III) ion excitation energies for the 4F to 2G transition. Two generate spin eigenfunctions are given for FD-DFT excitation energies (2-1-1 and 1-1). All energies are in eV.

Cr ³⁺ $^4F \rightarrow ^2G$	HF	B3LYP	B55LYP	APF-D	PBE1PBE	MN15	Exp ³¹
FD-DFT (SCF)(2-1-1)	2.94	1.97	2.22	2.04	2.08	1.83	1.81
FD-DFT (CI)(2-1-1)	2.94	2.03	2.26	1.95	2.14	2.14	
FD-DFT (SCF)(1-1)	2.96	1.97	2.23	2.06	2.08	1.87	
FD-DFT (CI)(1-1)	2.96	2.02	2.27	2.06	2.14	2.08	
Broken Symmetry	1.79	1.29	1.41	1.35	1.36	0.60	

$\alpha\beta\alpha - \beta\alpha\alpha$ (1-1) yield practically equivalent excitation energies under SCF, showing good stability and agreement with theory under different degenerate determinant combinations.

As evident from the data in Table 2.3 computing the 4F to 2G excitation energy in Cr(III) is challenging. The chromium core 3s and 3p orbitals are nearly the same size as the singly occupied valence 3d orbitals. This spatial similarity leads to significant 3p-3d electron correlation that is differential between the quartet and doublet states. This leads to functionals with less HF exchange to outperform those with higher HF exchange like Becke half and half with LYP exchange. Unlike previous functionals, MN15 excitation energies fall close to the experimental value, showing the inability of one functional to match all systems. Multiplet-derived exchange has not been incorporated in any exchange functional development yet. Like nitrogen atom, the two doublet states match closely for FD-DFT calculations, and the broken-symmetry calculations dramatically underestimate the excitation energy.

FIVE ELECTRON SYSTEMS Fe(III):

Iron containing photocatalysts are highly sought after as potential replacements for ruthenium based catalysts. While the electronic states of Fe and Ru based complexes may seem similar, Fe can occupy a large variety of potential electronic spin states due to presence of high and low spin capable d-orbitals whose relative energies are sufficiently perturbed the ligands. Therefore, reliable excitation energies are crucial to understanding Fe-based complexes potential as photocatalysts, especially with increasing ligand complexity. Five unpaired electrons allows for a wide range of multiplet states possible so good agreement with experimental results regarding the

absolute excitation energy as well as the relative ordering of the multitude of states is crucial.

The lowest quartet transition, ${}^6S \rightarrow {}^4G$, as well as the two lowest doublet transitions (${}^6S \rightarrow {}^2I$, ${}^6S \rightarrow {}^2D$) from the ground state sextet state are given in Table 2.4. All FD-DFT functional performs well at calculating excitation energies, compared to HF and broken symmetry methods for the quartet and doublet, falling within 0.5 eV for both the SCF converged and CI techniques. Again, Becke half-and-half with LYP correlation performs the best due to the increase in exact HF exchange. The FD-DFT doublet energies also agree well with experiment, and FD-DFT is effective at separating the two doublets. However, the magnitude of the error with respect to the experimental values is not consistent across different transitions and functionals. It is important to remember that these functionals were not optimized for the calculation of excited states or open-shell systems, but rather are tuned such that the best agreement with ground state closed shell calculations is achieved. It suggests that additional work is needed to develop functionals that can be more effectively applied to excited state calculations using FD-DFT.

CONCLUSIONS:

We have presented our new method, few-determinant density functional theory, which is designed to calculate excited states of molecular systems using restricted open shell concepts. The key advantage this method has over competing methods is the use of the minimum number of determinants needed to obtain the missing energies and potentials not present in single determinant wave functions. This not only reduces the computational burden compared to post Hartree-Fock methods, it also avoids double

Table 2.4: Fe(III) ion excitation energies for the quartet transition and two doublet transitions for FD-DFT and broken symmetry calculations. Only one broken symmetry doublet can be calculated while the two lowest doublets are provided for FD-DFT. All energies are in eV.

$\text{Fe}^{3+} \text{ } ^6\text{S} \rightarrow \text{ } ^4\text{G}$	HF	B3LYP	B55LYP	APF-D	PBE1PBE	MN15	Exp ³¹
FD-DFT (SCF)	4.98	3.44	3.80	3.61	3.65	4.16	4.00
FD-DFT (CI)	5.08	3.40	3.81	3.59	3.64	3.99	
Broken Symmetry	3.77	2.65	2.92	2.81	2.84	3.15	
Fe^{3+} Doublets							
FD-DFT (SCF) $^6\text{S} \rightarrow \text{ } ^2\text{I}$	7.54	5.19	5.70	5.45	5.50	7.75	5.84
FD-DFT (CI) $^6\text{S} \rightarrow \text{ } ^2\text{I}$	8.61	5.75	6.48	6.09	6.15	5.13	
FD-DFT (SCF) $^6\text{S} \rightarrow \text{ } ^2\text{D}$	8.43	5.80	6.44	6.09	6.15	5.41	6.17
FD-DFT (CI) $^6\text{S} \rightarrow \text{ } ^2\text{D}$	7.63	5.13	5.70	5.43	5.48	7.59	
Broken Symmetry	5.09	3.68	3.97	3.90	3.93	5.92	

counting of exchange and correlation terms that are already present in the DFT functionals. In addition, we have found the method to be stable under SCF iterations, which helps it produce better excitation energies even if the excited state wave function differs significantly from the ground state. The initial results on O, O₂, N, Cr³⁺, and Fe³⁺ give good indications that method can obtain useful results to compare to experiment. In addition, the low computational burden of the method gives promise that it can be applied to larger systems, which are too large for many post-HF methodologies.

REFERENCES

- (1) Noodleman, L.; Davidson, E. R. Ligand Spin Polarization and Antiferromagnetic Coupling in Transition Metal Dimers. *Chem. Phys.* **1986**, *109* (1), 131–143.
- (2) Miehlich, B.; Stoll, H.; Savin, A. A Correlation-Energy Density Functional for Multideterminantal Wavefunctions. *Mol. Phys.* **1997**, *91* (3), 527–536.
- (3) Soda, T.; Kitagawa, Y.; Onishi, T.; Takano, Y.; Shigeta, Y.; Nagao, H.; Yoshioka, Y.; Yamaguchi, K. Ab Initio Computations of Effective Exchange Integrals for H–H, H–He–H and Mn₂O₂ Complex: Comparison of Broken-Symmetry Approaches. *Chem. Phys. Lett.* **2000**, *319* (3), 223–230.
- (4) Filatov, M.; Shaik, S. Diradicaloids: Description by the Spin-Restricted, Ensemble-Referenced Kohn–Sham Density Functional Method. *J. Phys. Chem. A* **2000**, *104* (28), 6628–6636.
- (5) Ukai, T.; Nakata, K.; Yamanaka, S.; Takada, T.; Yamaguchi, K. A CAS-DFT Study of Fundamental Degenerate and Nearly Degenerate Systems. *Mol. Phys.* **2007**, *105* (19–22), 2667–2679.
- (6) Ángel J. Pérez-Jiménez; José M. Pérez-Jordá; Juan C. Sancho-García. Combining Two-Body Density Correlation Functionals with Multiconfigurational Wave Functions Using Natural Orbitals and Occupation Numbers. *J. Chem. Phys.* **2007**, *127* (10), 104102.
- (7) Kurzweil, Y.; Lawler, K. V.; Head-Gordon, M. Analysis of Multi-Configuration Density Functional Theory Methods: Theory and Model Application to Bond-Breaking. *Mol. Phys.* **2009**, *107* (20), 2103–2110.

- (8) Ying, F.; Su, P.; Chen, Z.; Shaik, S.; Wu, W. DFVB: A Density-Functional-Based Valence Bond Method. *J. Chem. Theory Comput.* **2012**, *8* (5), 1608–1615.
- (9) Ziegler, T.; Rauk, A.; Baerends, E. J. On the Calculation of Multiplet Energies by the Hartree-Fock-Slater Method. *Theor. Chim. Acta* **1977**, *43* (3), 261–271.
- (10) Hoffert, W. A.; Rappé, A. K.; Shores, M. P. Topological and Electronic Influences on Magnetic Exchange Coupling in Fe(III) Ethynylbenzene Dendritic Building Blocks. *J. Am. Chem. Soc.* **2011**, *133* (51), 20823–20836.
- (11) McDaniel, A. M.; Tseng, H.-W.; Hill, E. A.; Damrauer, N. H.; Rappé, A. K.; Shores, M. P. Syntheses and Photophysical Investigations of Cr(III) Hexadentate Iminopyridine Complexes and Their Tris(Bidentate) Analogues. *Inorg. Chem.* **2013**, *52* (3), 1368–1378.
- (12) Shao, Y.; Head-Gordon, M.; Krylov, A. I. The Spin-flip Approach within Time-Dependent Density Functional Theory: Theory and Applications to Diradicals. *J. Chem. Phys.* **2003**, *118* (11), 4807–4818.
- (13) Wang, F.; Ziegler, T. Time-Dependent Density Functional Theory Based on a Noncollinear Formulation of the Exchange-Correlation Potential. *J. Chem. Phys.* **2004**, *121* (24), 12191.
- (14) Frank, I.; Hutter, J.; Marx, D.; Parrinello, M. Molecular Dynamics in Low-Spin Excited States. *J. Chem. Phys.* **1998**, *108* (10), 4060–4069.
- (15) Pérez-Jiménez, A. J.; Moscardó, F.; Sancho-García, J. C.; Abia, L. P.; San-Fabián, E.; Pérez-Jordá, J. M. New Approach to the Design of Density Functionals. *J. Chem. Phys.* **2001**, *114* (5), 2022–2026.

- (16) Russo, T. V.; Martin, R. L.; Hay, P. J. Density Functional Calculations on First-Row Transition Metals. *J. Chem. Phys.* **1994**, *101* (9), 7729–7737.
- (17) Bobrowicz, F. W.; William A. Goddard III. The Self-Consistent Field Equations for Generalized Valence Bond and Open-Shell Hartree—Fock Wave Functions. In *Methods of Electronic Structure Theory*; III, H. F. S., Ed.; Modern Theoretical Chemistry; Springer US, 1977; pp 79–127.
- (18) Frisch, M. J.; Trucks, G. W.; Schlegel, H. B.; Scuseria, G. E.; Robb, M. A.; Cheeseman, J. R.; Scalmani, G.; Barone, V.; Petersson, G. A.; Nakatsuji, H.; et al. *Gaussian 16 Revision A.03*.
- (19) Mulliken, R. S. Interpretation of the Atmospheric Absorption Bands of Oxygen. *Phys. Rev.* **1928**, *32* (6), 880.
- (20) Charlotte E. Moore. *Selected Tables of Atomic Spectra: Atomic Energy Levels and Multiplet Tables OI*.
- (21) Higgins, R. F.; Fatur, S. M.; Shepard, S. G.; Stevenson, S. M.; Boston, D. J.; Ferreira, E. M.; Damrauer, N. H.; Rappé, A. K.; Shores, M. P. Uncovering the Roles of Oxygen in Cr(III) Photoredox Catalysis. *J. Am. Chem. Soc.* **2016**, *138* (16), 5451–5464.
- (22) Cen, J.; Wu, Q.; Liu, M.; Orlov, A. Developing New Understanding of Photoelectrochemical Water Splitting via In-Situ Techniques: A Review on Recent Progress. *Green Energy Environ.* **2017**, *2* (2), 100–111.
- (23) Moss, B. J.; Goddard, W. A. Configuration Interaction Studies on Low-lying States of O₂. *J. Chem. Phys.* **1975**, *63* (8), 3523–3531.
- (24) Racah, G. Theory of Complex Spectra. II. *Phys. Rev.* **1942**, *62* (9–10), 438–462.

- (25) Racah, G. Theory of Complex Spectra. III. *Phys. Rev.* **1943**, 63 (9–10), 367.
- (26) Ballhausen, C. J. *Introduction to Ligand Field Theory*; McGraw-Hill Inc.,US, 1962.
- (27) K. P. Huber; G. Herzberg. *Molecular Spectra And Molecular Structure, IV. Constants Of Diatomic Molecules.*
- (28) Juban, E. A.; McCusker, J. K. Ultrafast Dynamics of 2E State Formation in Cr(Acac)₃. *J. Am. Chem. Soc.* **2005**, 127 (18), 6857–6865.
- (29) Juban, E. A.; Smeigh, A. L.; Monat, J. E.; McCusker, J. K. Ultrafast Dynamics of Ligand-Field Excited States. *Coord. Chem. Rev.* **2006**, 250 (13–14), 1783–1791.
- (30) Charlotte E. Moore. *Selected Tables of Atomic Spectra: Atomic Energy Levels and Multiplet Tables NIV, NV, NVI, NVII*; National Bureau of Standards, 1970.
- (31) Sugar, J.; Corliss, C. *Atomic Energy Levels of the Iron-Period Elements: Potassium through Nickel*; Technical Report PB-86-165446/XAB; American Chemical Society: United States, 1985.

CHAPTER 3: TRIS(1,3-PROPANEDIONATO)CHROMIUM(III) FOR INSIGHT INTO Cr(III) BASED PHOTOCATALYSTS

INTRODUCTION:

The photophysical properties of transition metal complexes have been of great interest in the recent literature. Their increasing use as photocatalysts in classic organic reactions has presented novel solutions for green chemistry in industrial production of critical feedstocks as well as providing new reaction pathways for synthesizing alternative reaction products. The majority of transition metal photocatalytic research has focused on Ru based complexes, however, the rarity of the material inhibits wide spread use, fiscally. New efforts in the literature to replace ruthenium-based catalysts have been successful, but first row transition metal photocatalysts are not without significant challenges compared to their heavy metal counterparts.

The complications involved in using first-row transition metal complexes are directly related to the significant difference in the photophysical properties between second and third-row transition metals and their first-row equivalents. For example, for the ubiquitous tris(bipyridine)ruthenium(II) ($\text{Ru}(\text{bpy})_3^{2+}$) a well defined excited state manifold is observed in which the primary excitation is metal to ligand charge transfer. The stable excited state is spin-orbit coupling perturbed triplet, which provides relatively long lifetime as the transition back to the singlet ground state is classically forbidden. In comparison, first-row complexes exhibit a wide variety of stable ground and excited state configurations depending on ligands and environmental conditions. The excited state manifolds are complicated and don't follow the general trends seen in organic and

heavier transition metal complexes. Juban and McCusker found that Cr(III)(AcAc)_3 exhibited intersystem crossing (ISC) rates that exceeded the vibrational cooling (VC) rates, eschewing the traditional hierarchy of VC, followed by ISC, followed by phosphorescence.¹ The uniqueness of the excited state dynamics of Cr(III)(AcAc)_3 has increased the research efforts into understanding the photophysics of chromium based and other first-row transition metal complexes.²

The excitation pathway of Cr(III)(AcAc)_3 is difficult to precisely define since it does not follow the cascade model of vibrational cooling, then internal conversion, then intersystem crossing in terms of increasing time scale. The ground state of the complex is the $^4A_{2g}$ state. Upon excitation, it populated the $^4T_{2g}$ state. From here, VC and ISC compete such that the exact pathway isn't completely understood. After the ISC, VC, and IC events, the complex relaxes to the 2E_g state. This state is the long lived state for many octahedrally coordinated Cr(III) complexes by which the complex can act catalytically.¹

Theorists have also been interested in studying the photophysics of Cr(III)(AcAc)_3 complexes, not only to confirm the experimentally observed phenomenon, but also to help understand the unique excited state characteristics of the complex. As new theoretical methods for excited state systems have been developed, they have been applied to Cr(III)(AcAc)_3 systems to be better understand them.^{3,4} While many efforts have centered around the use of perturbation theory calculations based on multiconfiguration self consistent field (MCSCF) wave functions, the latest theoretical results from Ando et al. on the Cr(III)(AcAc)_3 system used multiconfigurational quasidegenerate perturbation theory (MCQDPT) theory to calculate excited state

potential energy surfaces along the path from the $^4A_{2g}$ geometry to the distorted $^4T_{2g}$ geometry.⁵ The authors calculated the distorted state by constraining the structure to the C_2 symmetry point group and calculating the wave function of orthogonal symmetry to the ground state wave function. They found that the initial excited state $^4T_{2g}$ curve does cross the 2E_g curve, but determined that the spin orbit coupling (SOC) was weak between the states. Instead they claimed that transition to the $^2T_{1g}$ was a more likely ISC pathway with an internal conversion to the lower 2E_g state. It should be noted that the computed energy gap between the $^4T_{2g}$ and 2E_g states was smaller than that experimentally observed, and it is unknown whether that contributed to additional crossing between the two states along the distortion path.

The work presented here contains a few differences in an attempt to gain insight into these $Cr(III)(AcAc)_3$ systems. First, it focuses on a derivative of $Cr(III)(AcAc)_3$, tris(1,3-propanedionato)chromium(III) ($Cr(III)(PDO)_3$). The PDO is closely related to the AcAc ligand in that the methyl groups in the AcAc ligand have been removed to allow for higher level computational methods to be employed. Second, the excited state of the $Cr(III)$ complex is optimized to a structure where the second derivatives with respect to atomic displacement were positive, resulting in an excited state structure with real vibrational frequencies. This ensures the excited state structure is at a true minimum. Lastly, a configuration interaction (CI) method, spectroscopy oriented configuration interaction (SORCI) method, was used to calculate the excited state manifold.

The SORCI method, developed by Frank Neese's research group, was designed to overcome challenges faced by traditional CI methods.⁶ The method focuses on including differential electron correlation terms that are associated with the excitation

process rather than terms associated with the absolute energies of the excited states. This is accomplished by three important improvements to traditional CI methods: use of a difference dedicated CI to obtain the excitation energies, combined use of perturbation theory with variational CI, and a reduction of the CI space. The difference-dedicated CI is key to obtaining excitation energies that match experimental values because it removes error terms from the CI wave functions that cancel when subtracted.^{7,8} The combined use of CI with Møller–Plesset perturbation theory improves the energy of each state in the CI expansion while the variational aspect of the CI removes any intruder state problems. The method also takes care to reduce the CI space needed whenever possible to allow for an appropriate number of CI states to be included to reproduce the correct wave function while keeping computational requirements low.

The use of a CI calculation also allows for the inclusion of spin-orbit coupling contributions to be included in the calculation. In the absence of a strong magnetic field, first-row transition metal complexes exhibit coupling between the spatial orbital angular momentum \mathbf{L} and the spin orbital angular momentum \mathbf{S} .⁹ The magnitude of the coupling can be represented by the equation

$$H_{\text{SOC}} = \lambda \mathbf{L} \cdot \mathbf{S} \quad (0.1)$$

where H_{SOC} is the spin-orbit operator that couples states that differ in angular momentum and spin, λ is the magnitude of the spin orbit coupling.⁹ The importance of the inclusion of spin-orbit coupling in the calculation is that spin-orbit coupling effects can provide an avoided crossing between the two potential energy surfaces since states of different spatial orbital and spin may share the same total spin-orbit. This would allow

for an avoided crossing between the $^4T_{2g}$ and the 2E_g states, which would allow for a fast ISC event. The magnitude of the coupling between states near the crossing of these surfaces would provide evidence for a pathway between the quartet and doublet states.

The goals of this paper are to compare accuracy of the SORCI method compared to previously cited approaches in the literature as well as map out the most likely excited state relaxation pathway to help understand the extreme dynamics present in the Cr(III)(AcAc)₃ type systems.

COMPUTATIONAL METHODS:

STRUCTURE OPTIMIZATIONS:

The structures of the Cr(III)(AcAc)₃ and Cr(III)(PDO)₃ complexes $^4A_{2g}$ ground state were optimized with the APF-D functional with the cc-pVTZ basis set. The structure for the $^4A_{2g}$ ground state was also used to represent the 2E_g state, since the structures are quite similar given the shared t_{2g} electronic configuration. The $^4T_{2g}$ excited state structure for Cr(III)(PDO)₃ was calculated by promoting an electron from the t_{2g} orbitals to the e_g orbitals while forcing the molecular symmetry to be restricted to the C_2 point group. The resulting change in wave function symmetry under excitation locked the wave function to this orthogonal state, and the structure was allowed to optimize under C_2 symmetry. This resulted in a structure previously found in literature.⁵ Additionally, the excited state was allowed to continue optimizing without the C_2 restriction until the second derivatives with respect to atomic displacement were positive, resulting in a structure not belonging to the C_2 point group. This structure is referred to as the vibrational minimum structure. This structure was 0.018 eV lower than

the C₂ optimized structure and was used as the ⁴T_{2g} structure for the following calculations. All optimization calculations were performed using the Gaussian09 electronic structure software suite.¹⁰

REACTION PATHWAY:

For the pathway between the ²E_g and ⁴T_{2g} states, a linearly interpolated path was chosen following the method of Miller et al.¹¹ The specific details are in Chapter IV. Briefly, the ²E_g and ⁴T_{2g} states were aligned such that there existed no net linear or angular momentum between the structures. The condition of no linear momentum was accomplished by translating each structure to their center of masses. The angular momentum constraint was satisfied by numerically solving for the Euler indices that satisfy the equation $\sum_i m_i (\vec{R}_i^r \times \vec{R}_i^p) = 0$. Intermediate structures between the optimized ²E_g and ⁴T_{2g} were generated by linear interpolation.

FD-DFT CI:

The few-determinant density functional theory (FD-DFT) method was also applied to both the Cr(III)(AcAc)₃ and Cr(III)(PDO)₃ systems. The methodology of this theoretical method is described in detail in Chapter II. The FD-DFT CI energies of AcAc and PDO based Cr(III) complexes were calculated using the APF-D functional and the basis sets 6-311+G(D) and cc-pVTZ for the Cr(III)(PDO)₃ and Cr(III)(AcAc)₃ structures respectively. Only the ²E_g was calculated using the FD-DFT method due to the limitation of the current implementation of FD-DFT in which only open-shell multiplets states are correctly described. All FD-DFT calculations were performed using the Gaussian16 software package suite using a in-house modified GVB module.¹²

SORCI:

The excited state energies for the $^4A_{2g}/^2E_g$, $^4T_{2g}$, and all intermediate structures were calculated with the SORCI method. The starting guess for the SORCI wave function was obtained by a two-step process. Initially, a DFT wave function was calculated using the B3LYP functional. This wave function was used as the initial guess for a complete active space self-consistent field (CASSCF) calculation using a state-averaged 3,5 active space. This active space was chosen to capture sufficient character of the d orbitals on the chromium metal center for the multiconfiguration wave function.

The CASSCF wave function was used as the wave function for a SORCI calculation. The SORCI calculation included additional core electrons by including core orbitals less negative than 4 Hartree, this corresponds to the Cr 3p orbitals. The lower bound by which core orbitals were included was determined by comparing the SORCI energies to Cr(III) ion experimental excitation energies. The SORCI results were used to calculate the excitation energies relative to the ground state as well as the spin state of each excited state. This was performed for each geometry along the linear reaction pathway. The DFT, CASSCF, and SORCI calculations used the cc-pVDZ basis set without polarizing functions on the hydrogen atoms plus the cc-pCVTZ basis set on the Cr atom to insure the core orbitals could obtain the proper shape when included in the CI expansion.

For structures that exhibited significant crossing of states along the distortion path, additional SORCI calculations were performed that allowed for spin orbit coupling contributions to the wave function to be included. This allowed states that exhibited mixed spin state character to be identified. The inclusion of spin-orbit coupling effects

into the CI wave function adds additional computational time, so the SOC contributions were only included in the region of $R = 0.5$ to 0.75 where significant crossings of the potential energy curves were found. All SORCI related calculations were performed using the ORCA electronic structure software package version 3.0.3.¹³

RESULTS:

The excitation energies obtained from the SORCI calculations for the PDO and AcAc complexes compare favorably to previous calculations of Cr(III)(AcAc)_3 as well as experimental values. The SORCI excitation energies for the 2E_g state have much better agreement with experimental values (1.65 eV vs. 1.94 eV) while the perturbative approach more accurately reflects the experimental ${}^4T_{2g}$ state (2.42 eV vs. 2.27 eV).^{3,5,14-16} The FDDFT excitation values are closest in agreement with experimental values, falling within hundredths of an electron volt. This highlights the complexity of accurately modeling these complexes even when utilizing current state of the art methodologies as no single method can reproduce the excitation energies of both the ${}^4T_{2g}$ and 2E_g state simultaneously. Interestingly, the SORCI and MCQDPT approaches change the energy gap between the ${}^4T_{2g}$ and 2E_g states. As expected, the modification of the AcAc ligand to the PDO ligand minimally impacts the excitation energy of these metal center d-d transitions for both the ${}^4T_{2g}$ ($\Delta E = 0.31$ eV) and 2E_g ($\Delta E = 0.072$ eV) states as has been previously noted in literature using other methods.³ The excited state excitation energies for the ${}^4A_{2g}$ state are listed in Table 3.1.

The SORCI excitation energies along the ${}^4A_{2g}$ to ${}^4T_{2g}$ structural distortion provide a look into the possible pathway for the fast ISC crossing process (See Figure 3.1). Multiple crossings are observed between the lowest quartets with the doublet starting at

Table 3.1: Excitation energies for the ${}^4A_{2g}$ geometry for the AcAc and PDO ligands in Cr(III) complexes for various methods. All energies are in eV.

	${}^4T_{2g}$	2E_g
Cr(III)(AcAc) ₃		
SORCI	2.42	1.65
MCQDPT ⁵	2.27	1.94
FD-DFT CI	-	1.62
Experimental ^{3,14-16}	2.26	1.62
Cr(III)(PDO) ₃		
SORCI	2.73	1.72
FD-DFT CI	-	1.59
CASPT2 ³	2.10	1.93

R = 0.6. Similar excited state behavior was noticed by Ando et al. with the crossing computed with MCQDPT occurred at R = 0.45 for the crossing between the ${}^4T_{2g}$ and the 2E_g . The two final distorted structures (the C_2 symmetry constrained vibrational minimum) both exhibited crossing at similar points along the linear reaction path. The SORCI and MCQDPT methods for calculating the excited states both give relatively similar crossing points that are thought to lead to the ISC event in these complexes despite the large difference in the relative positions of the quartet and doublet state manifolds of interest as well as differences in the ligands. In addition, similar conclusions can be drawn from the curves where the endpoint structures of the linear pathways are separate structures.

The spin orbit coupling contributions to the SORCI calculations provide additional insight into the excited state pathways of the Cr(III)(PDO)₃ complex. As can be seen in Figure 3.2, the quartet and doublet states at the region of crossing exhibit a great deal of mixed character. Focusing just on the region between 2.3 eV and 2.9 eV, the states which form closer to 50:50 doublet/quartet character form a vertical avoided crossing into the doublet states. Since this pathway is completely downhill energetically, an

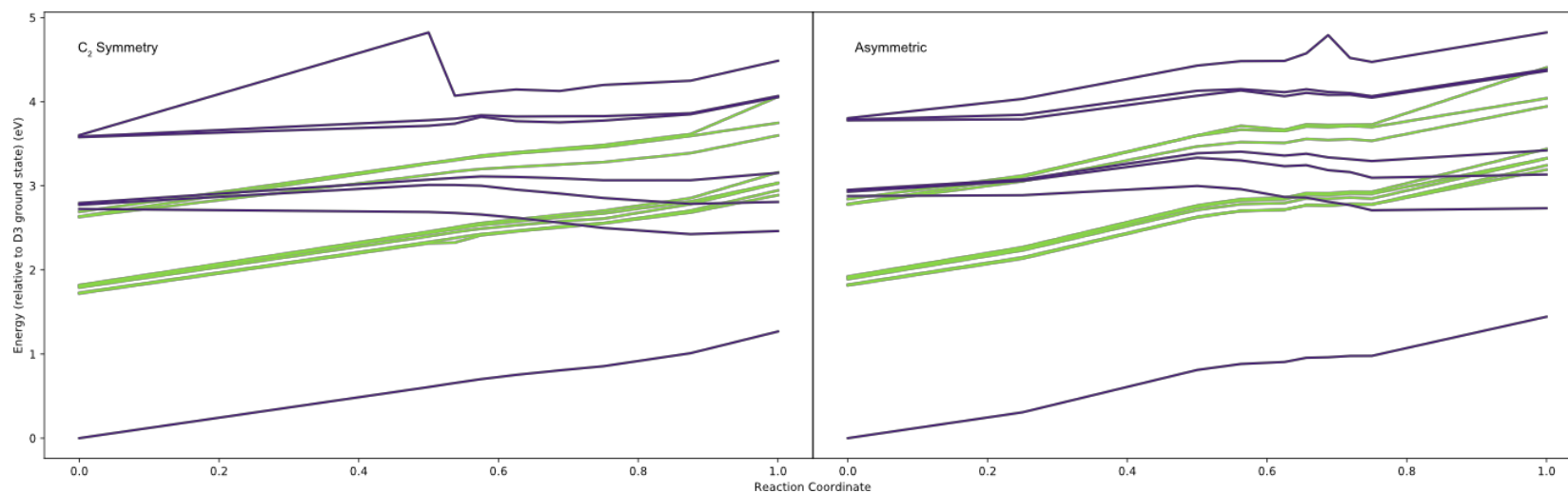


Figure 3.1: SORCI calculations for the linear reaction path between the $^4A_{2g}$ and $^4T_{2g}$ geometries for the C_2 symmetry and vibrational minimum distorted structures. The purple lines represent the quartet states and the green lines represent the doublet states.

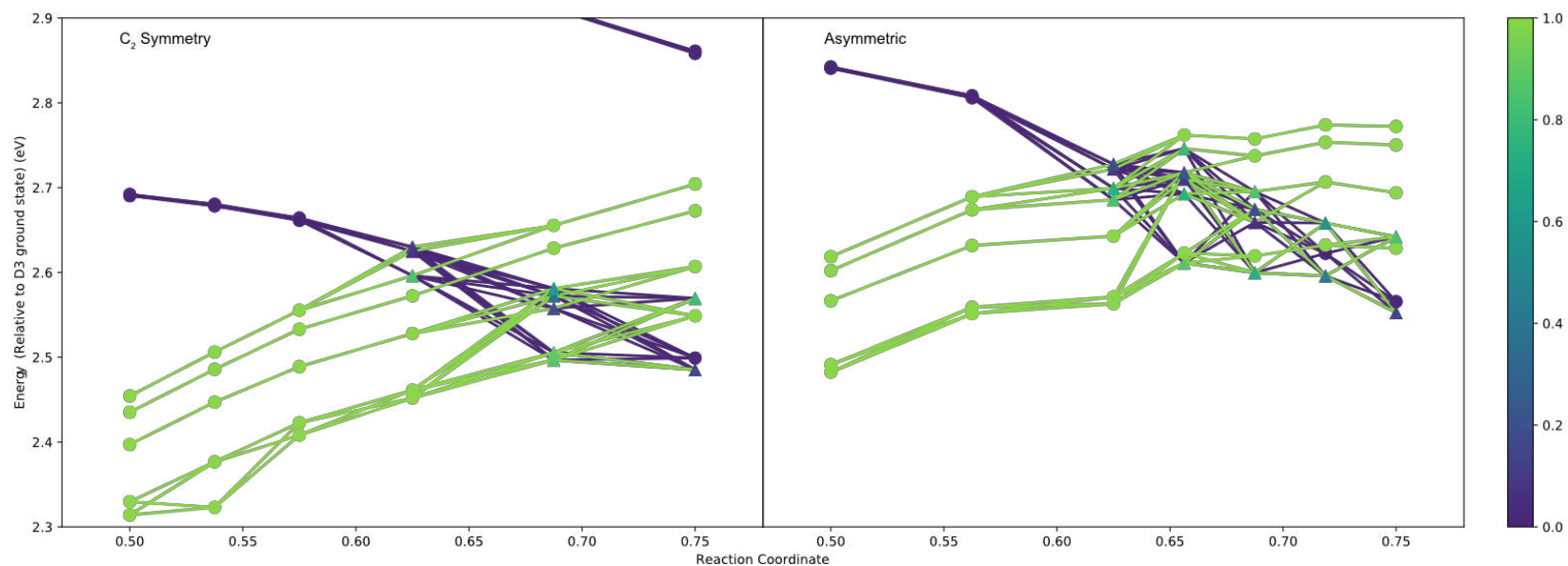


Figure 3.2: SORCI excited state calculations including SOC contributions for the reaction coordinate range 0.5 to 0.75 for the linear paths formed from the C_2 constrained structure and the vibrational minimum structure. The y-axis range has been limited to 2.3-2.9 eV for better clarity in the lowest crossing region. The lines are colored purple for quartet states and green for doublet states. Each circle represents a pure doublet/quartet state while the triangles represent a state of mixed character whose mixture corresponds to the color bar.

avoided crossing would result in a fast ISC rate, which agrees with previous experimental work and theory.^{1,5}

While the SOC mixing picture provides a qualitative pathway to the final 2E_g state, the exact states which are most likely to be involved in the ISC were extracted from the SOC calculations. We find that not only do the ${}^4T_{1g}$ states have large SOC splittings, which is indicative of strong SOC between states due to Eq. (0.1), we find that the ${}^4T_{2g}$ to 2E_g transition has splitting energies over 250 cm^{-1} RMS along the path, compared to 21 cm^{-1} previously reported.⁵ We theorize that many paths are taken since the ${}^2T_{1g}$ and 2E_g exhibit spin orbit coupling amongst themselves near the mixing region. While the main path may be the previously suggested ${}^4T_{2g} - {}^2T_{1g} - {}^2E_g$, the direct ${}^4T_{2g} - {}^2E_g$ path is not as improbable as previously thought.

CONCLUSIONS:

The SORCI calculations presented here effectively reproduce the behavior exhibited by both the experimental and theoretical results previously published. It is of particular interest that the crossing of excited state energies and spin orbit coupling between the states is still observed when using substantially different theoretical approaches and structures. An energy gap between excited states that is larger than experimental observed still results in clear spin orbit coupling between the excited states. This helps support the use of similar techniques on other complexes without concerns of interpretation consistency when using different theoretical methods.

REFERENCES

- (1) Juban, E. A.; McCusker, J. K. *J. Am. Chem. Soc.* **2005**, *127* (18), 6857–6865.
- (2) Juban, E. A.; Smeigh, A. L.; Monat, J. E.; McCusker, J. K. *Coord. Chem. Rev.* **2006**, *250* (13–14), 1783–1791.
- (3) Ribbing, C.; Pierloot, K.; Ceulemans, A. *Inorg. Chem.* **1998**, *37* (20), 5227–5232.
- (4) Neese, F. *J. Am. Chem. Soc.* **2006**, *128* (31), 10213–10222.
- (5) Ando, H.; Iuchi, S.; Sato, H. *Chem. Phys. Lett.* **2012**, *535*, 177–181.
- (6) Neese, F. *J. Chem. Phys.* **2003**, *119* (18), 9428–9443.
- (7) Miralles, J.; Daudey, J.-P.; Caballol, R. *Chem. Phys. Lett.* **1992**, *198* (6), 555–562.
- (8) Miralles, J.; Castell, O.; Caballol, R.; Malrieu, J.-P. *Chem. Phys.* **1993**, *172* (1), 33–43.
- (9) Eisberg, R.; Resnick, R. *Quantum Physics of Atoms, Molecules, Solids, Nuclei, and Particles*, 2nd edition.; John Wiley & Sons: New York, 1985.
- (10) Frisch, M. J.; Trucks, G. W.; Schlegel, H. B.; Scuseria, G. E.; Robb, M. A.; Cheeseman, J. R.; Scalmani, G.; Barone, V.; Mennucci, B.; Petersson, G. A.; Nakatsuji, H.; Caricato, M.; Li, X.; Hratchian, H. P.; Izmaylov, A. F.; Bloino, J.; Zheng, G.; Sonnenberg, J. L.; Hada, M.; Ehara, M.; Toyota, K.; Fukuda, R.; Hasegawa, J.; Ishida, M.; Nakajima, T.; Honda, Y.; Kitao, O.; Nakai, H.; Vreven, T.; Montgomery, Jr., J. A.; Peralta, J. E.; Ogliaro, F.; Bearpark, M.; Heyd, J. J.; Brothers, E.; Kudin, K. N.; Staroverov, V. N.; Kobayashi, R.; Normand, J.; Raghavachari, K.; Rendell, A.; Burant, J. C.; Iyengar, S. S.; Tomasi, J.; Cossi, M.; Rega, N.; Millam, J. M.; Klene, M.; Knox, J. E.; Cross, J. B.; Bakken, V.; Adamo,

C.; Jaramillo, J.; Gomperts, R.; Stratmann, R. E.; Yazyev, O.; Austin, A. J.; Cammi, R.; Pomelli, C.; Ochterski, J. W.; Martin, R. L.; Morokuma, K.; Zakrzewski, V. G.; Voth, G. A.; Salvador, P.; Dannenberg, J. J.; Dapprich, S.; Daniels, A. D.; Farkas, Ö.; Foresman, J. B.; Ortiz, J. V.; Cioslowski, J.; Fox, D. J. *Gaussian 09 Revision D.01*.

(11) Miller, W. H.; Ruf, B. A.; Chang, Y.-T. *J. Chem. Phys.* **1988**, *89* (10), 6298–6304.

(12) Frisch, M. J.; Trucks, G. W.; Schlegel, H. B.; Scuseria, G. E.; Robb, M. A.; Cheeseman, J. R.; Scalmani, G.; Barone, V.; Petersson, G. A.; Nakatsuji, H.; Li, X.; Caricato, M.; Marenich, A. V.; Bloino, J.; Janesko, B. G.; Gomperts, R.; Mennucci, B.; Hratchian, H. P.; Ortiz, J. V.; Izmaylov, A. F.; Sonnenberg, J. L.; Williams-Young, D.; Ding, F.; Lipparini, F.; Egidi, F.; Goings, J.; Peng, B.; Petrone, A.; Henderson, T.; Ranasinghe, D.; Zakrzewski, V. G.; Gao, J.; Rega, N.; Zheng, G.; Liang, W.; Hada, M.; Ehara, M.; Toyota, K.; Fukuda, R.; Hasegawa, J.; Ishida, M.; Nakajima, T.; Honda, Y.; Kitao, O.; Nakai, H.; Vreven, T.; Montgomery, Jr., J. A.; Peralta, J. E.; Ogliaro, F.; Bearpark, M.; Heyd, J. J.; Brothers, E.; Kudin, K. N.; Staroverov, V. N.; Keith, T. A.; Kobayashi, R.; Normand, J.; Raghavachari, K.; Rendell, A. P.; Burant, J. C.; Iyengar, S. S.; Tomasi, J.; Cossi, M.; Millam, J. M.; Klene, M.; Adamo, C.; Cammi, R.; Ochterski, J. W.; Martin, R. L.; Morokuma, K.; Farkas, Ö.; Foresman, J. B.; Fox, D. J. *Gaussian 16 Revision A.03*.

(13) Neese, F. *Wiley Interdiscip. Rev. Comput. Mol. Sci.* **2012**, *2* (1), 73–78.

(14) Fatta, N. M.; Lintvedt, R. L. *Inorg. Chem.* **1971**, *10* (3), 478–481.

(15) Schönherr, T.; Eyring, G.; Linder, R. *Naturforsch* **1983**, *38*, 736–739.

(16) Atanasov, M. A.; Schönherr, T.; Schmidtke, H.-H. *Theor. Chim. Acta* **1987**, *71* (1), 59–73.

CHAPTER 4: UNDERSTANDING Cr(III) PHOTOCATALYSTS QUENCHING BY O₂

INTRODUCTION:

The increased use of tris(bipyridine)ruthenium(II) (Ru(II)(bpy)₃) catalysts to perform classic organic reactions has seen new research into finding earth abundant replacements for ruthenium.¹⁻⁷ Chromium based catalysts have shown potential as a suitable replacement for Diels alder reactions, bring unique and useful advantages beyond relative availability.⁸ The increased complexity of the excited states of these chromium-based catalysts allows for advantageous photocatalytic characteristics while making mechanistic studies challenging. For example, the catalyzed Diels Alder cycloaddition using Cr(III)(Ph₂phen)₃ was found to have O₂ playing a significant role in the mechanism through competitive quenching of the Cr photocatalyst.^{8,9} Understanding and modeling this quenching theoretically is crucial to studying these catalysts in real reactions.

The mechanism of the quenching by O₂ is has been suggested to occur via a spin conserving energy transfer between an excited Cr(III) complex in the long lived ²E state and O₂ in the ³Σ ground state.^{9,10} The transfer results in the Cr(III) catalysts returning to the ground state and the excitation of O₂ to the ¹Σ excited state. The ¹Σ state of O₂ is unstable and relaxes down the ¹Δ excited state, which is the dominant form of singlet O₂ in reactions. The ¹Δ O₂ species can then go on to perform other roles in the Diels Alder mechanism. The mechanistic scheme can be seen in Figure 4.1.

Theoretical studies of this mechanism are complicated by the spin states present in this system. While the spin states in Figure 4.1 represent these states as single spin

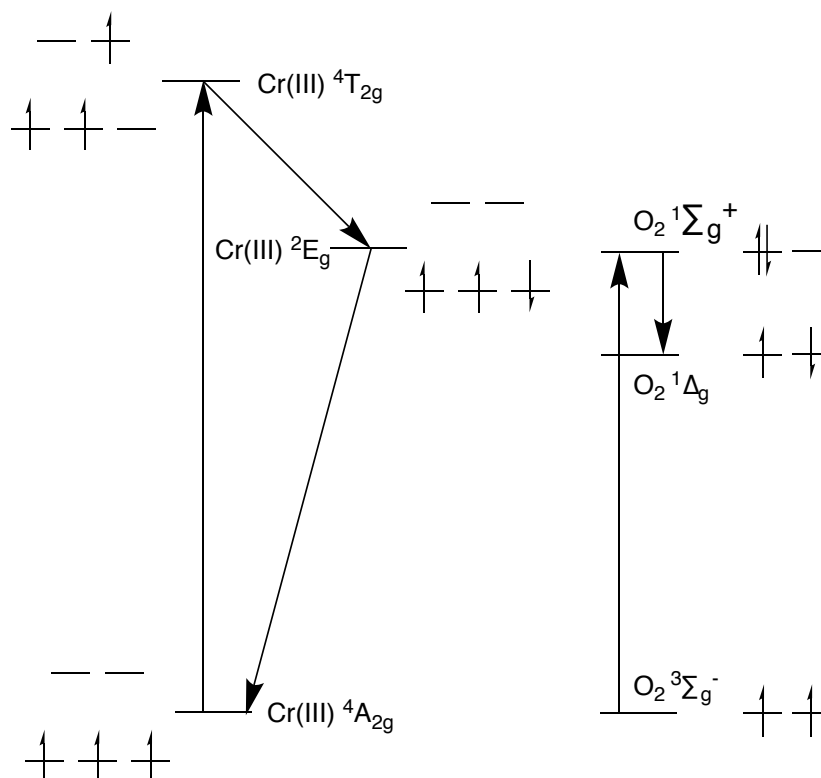


Figure 4.1: Reaction scheme for the quenching of chromium (III) based catalysts with O_2 . The interaction of the chromium complex in the $2E_g$ state excites the O_2 molecule up to the $1\Sigma_g^+$ state, quenching the chromium complex. The spin configuration for each state is given next to transition.

functions, the true spin eigenfunctions consist of multiple spin determinants for states that aren't the ground state sextet, which is a combination of the chromium $4A_{2g}$ state and 3Σ oxygen state. This is a particular problem for methods like standard Hartree-Fock and DFT, which are defined in terms of a single determinant. Previous theoretical studies have studied the Cr(III) based catalyst with O_2 system with DFT¹¹ as well as complete active space self consistent field (CASSCF) with second order n -electron valence state perturbation theory (NEVPT2).⁹ However, a DFT approach should not be able to properly represent the excitations, yet obtains results that suggest the same excited state, the $2E$, couples the Cr(III) complex to the O_2 molecule.

In order to elucidate the nature of the excited states of the combined

Cr(III)(PDO)₃•O₂ system, we compared both DFT and NEVPT2 approaches to understand why the DFT approach gives rise to a quartet state that isn't representable with a single determinant. We have chosen to use the tris(1,3-propanedionato)chromium(III) (Cr(III)(PDO)₃) complex as our Cr(III) complex due to its similar experimental excitation energies to Chromium(III) acetylacetonate as well as being computationally less time consuming. We have also included the few-determinant density functional theory (FD-DFT) method to compare to single determinant DFT to evaluate whether the DFT method with a proper multi-determinant treatment can replicate the NEVPT2 level of theory with less computational cost.

COMPUTATIONAL METHODS:

The structure of the Cr(III)(PDO)₃•O₂ system was calculated for the sextet ground state using DFT with the APF-D functional and the 6-311+G(D) basis set. The Cr – O₂ distance converged to a van der Waals complexed 3.66 Å. This structure was used for all subsequent calculations on the system. The lowest quartet and doublet states energies were calculated using the same approach as the optimization, but also employed a SCF stability check to ensure the lowest energy quartet and doublet states were obtained. These calculations were performed using the Gaussian09d software package suite.¹²

NEVPT2 calculations were performed on the Cr(III)(PDO)₃•O₂ system. The initial wave function guess was obtained using DFT with the B3LYP functional. This wave function was used as the starting guess for a state-averaged CASSCF calculation with a 9,9 active space. The active space was chosen to include the d-orbitals on the Cr(III)(PDO)₃ complex as well as the π and π^* orbitals on the O₂ molecule. The basis

set used for all NEVPT2-related calculations was the cc-(p)VDZ basis set, where all atoms except hydrogen have additional polarizing functions d, for all atoms except chromium where the cc-pCVTZ basis set was used. All NEVPT2 related calculations were performed using the ORCA program suite version 3.0.3.¹³

The FD-DFT calculations (described in Chapter II) were performed on the $\text{Cr(III)(PDO)}_3 \bullet \text{O}_2$ with the APF-D functional and 6-311+G(D). The initial guess for the FD-DFT calculations was obtained by calculating the restricted open shell wave function using the same DFT functional and basis set and the restricted open shell Kohn Sham method.¹⁴ The FD-DFT CI excitation energies were obtained for all 32 possible states for 5 singly occupied orbitals. All FD-DFT related wave functions and energies were performed using the Gaussian 16 suite of programs with a in-house modified GVB routine.¹⁵

RESULTS:

The results of the calculations help us understand the states present in this system as well as look at why certain methods get the excitation energies wrong (See Table 4.1). The NEVPT2 calculation correctly models the Heisenberg ladder that makes up the first doublet/quartet/sextet states with the doublet being the lowest. In addition, it also correctly calculates the first excited state above the Heisenberg ladder, and achieves good agreement with experiment.

The single determinant DFT calculations poorly estimate the excitation energies. The quartet state within a Heisenberg spin ladder is significantly higher than expected. The first excited quartet state energy is more than 0.45 eV above the ground state, while the doublet is 0.001 eV above the sextet. In addition to being counter to

Table 4.1: Cr(III)(PDO)₃ • O₂ excitation energy comparison for several theoretical methods. The excitation energies are all relative to the lowest sextet state. All excitation energies are in eV.

	DFT	FD-DFT	CASSCF	NEVPT2
Heisenberg Quartet	4.50e-1	1.76e-1	-6.00e-5	-1.70e-4
Heisenberg Doublet	1.18e-3	2.94e-1	-8.00e-5	-2.70e-4
¹ Δ O2 (Quartet)	-	9.44e-1	7.87e-1	1.07
² E Cr(III)(PDO) ₃ • O ₂ (Quartet)	-	1.72	1.50	1.96

experimental intuition, it is much higher than what other methods predict. The order of the Heisenberg ladder is out of order for the single determinant calculations compared to the CAS and NEVPT2 calculations, highlighting the need for more sophisticated methods to describe these states adequately.

The FD-DFT CI excitation energies are a mixture in terms of correlating with experiment and perturbation theory. Like the single determinant DFT calculations, the FD-DFT energies for the Heisenberg ladder states are out of relative order and overestimated. The combination of determinants used to calculate the quartet and doublet Heisenberg ladder states are similar to those used in the CAS wave function, but the requirement of the current FD-DFT implementation to have orthogonal open-shell orbitals prevents the FD-DFT excitation energies from having the proper state ordering.

Spin density plots were constructed for a number of excited states using the DFT and CASSCF calculations. The spin density plots were calculated using an iso value of 0.003. Only the DFT and CASSCF calculations provides spin density plots since the NEVPT2 only improves the energies of the CASSCF excitations with the orbitals remaining unchanged. Meanwhile, FD-DFT implemented in the GVB framework does not consider separate α and β spins. However, the excited states for both FD-

DFT and NEVPT2 were correlated with the CASSCF states by analyzing the determinantal composition of the CASSCF states. All spin density plots were generated using the Gausview visualization package version 6.0.1.2.

Looking at the spin density of the DFT and CASSCF calculations for the Heisenberg ladder states highlights the inadequacies with using single determinant methods to describe these states. The sextet spin densities look similar, however this is the only state where the spin eigenfunction is a single determinant (See Figure 4.2). For the doublets, the spin density plots are similar, but the densities are contracted for the CAS case, giving rise to the slight difference in energy. The largest discrepancy comes

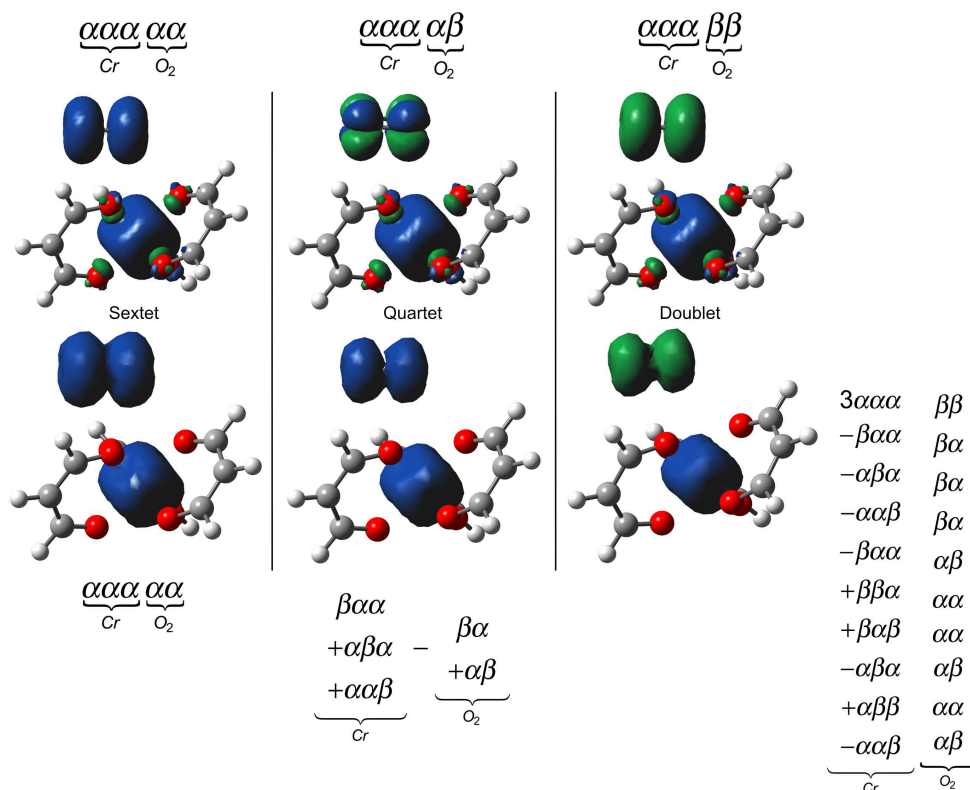


Figure 4.2: Spin density plots for the Heisenberg ladder states for $\text{Cr(III)(PDO)}_3 \cdot \text{O}_2$ generated from single determinant DFT and CASSCF calculations. The blue and green surfaces represent the unpaired α and β spin densities respectively. For each state and method combination, the spin determinants combinations are given.

from the quartet Heisenberg states, where DFT spin density for the quartet state has broken symmetry on O₂ molecule compared to the CAS state that displays a triplet O₂. This higher order wave function structure on the O₂ is the cause of the 0.45 eV increase in DFT excitation energy for the Heisenberg quartet over the other CAS based methods. This is in contrast to previous studies based on DFT calculations that claimed this Heisenberg quartet state is the active excited state in photocatalytic processes since its energy was found to be approximately 0.56 eV.¹¹ Great care must be taken to make sure that the method being employed can correctly model the systems being studied, otherwise theory being used for systems too complex for the theory to handle can lead to erroneous assignment of states. The determinants included in the CASSCF quartet suggest a Cr(III) $M_s = \frac{1}{2}$ quartet coupled with a O₂ $M_s = 0$ triplet state.

While the Heisenberg ladder states are a useful benchmark to exemplify the reason why single reference methods are inadequate for these systems, the interesting states involved in the quenching of Cr(III)(PDO)₃ by O₂ are in the 1-2 eV range. Experimentally, the ²E_g state of Cr(III)(AcAc)₃ like complexes and the ¹Σ_g state of O₂ are both around 1.5 eV, these are the states that are expected to be mixed to result in Cr(III) quenching. The excited states representing this mixed ²E state is found for FD-DFT, CASSCF, and NEVPT2 as shown in Table 4.1. All three methods get approximate values of this state, but do have a wide 0.4 eV range in excitation energies. In addition, the total system state comprised of the ¹Δ_g state of O₂ coupled with the ⁴A_{2g} state of Cr(III)(PDO)₃ is also found in the NEVPT2, CASSCF, and FD-DFT calculations.

The spin density plots of these states provide additional insight into why the mixed ²E state is where the quenching occurs. Looking at the CASSCF excited states

that represent the $^1\Delta$ and $^1\Sigma$, states we see only symmetric α density on the chromium metal center, suggesting that we are seeing only an excitation on the O_2 molecule (See Figure 4.3). These states would not support an energy transfer between the complex and the O_2 since the state by which the O_2 and $Cr(III)(PDO)_3$ transfer energy must couple the states together. However, the 2E states do show electron density on both the O_2 and the Cr complex. The most interesting of these states involves the first 2E state shown in Figure 4.3 where we see β electron character on the complex. This β electron surface is much smaller than would be expected for a localized beta electron in the t_{2g} orbitals on the metal center, and suggests that spin is reduced by coupling to the O_2 . This state would support spin transfer between the O_2 and $Cr(III)(PDO)_3$ complex.

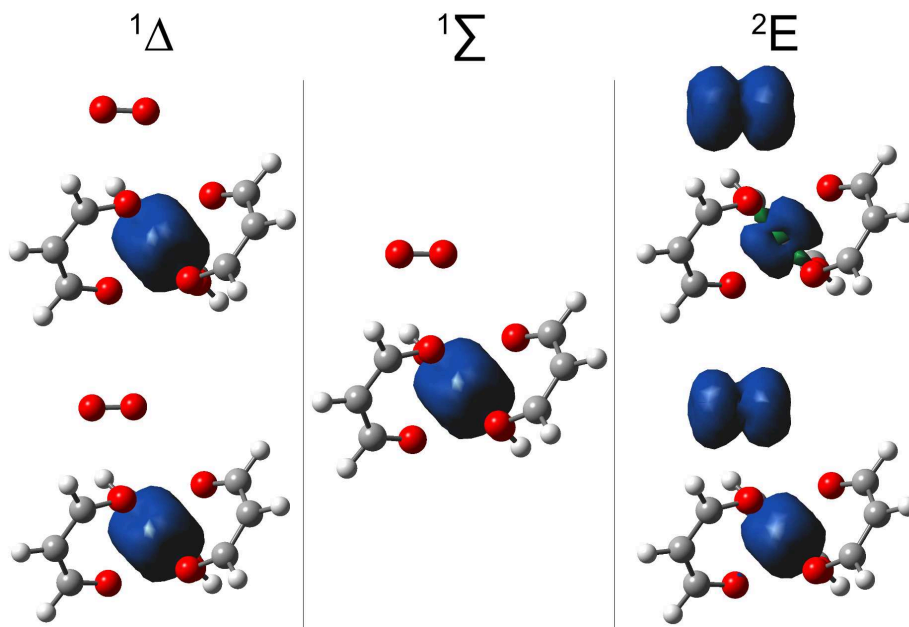


Figure 4.3: Spin density plots for the excited quartet states for $Cr(III)(PDO)_3 \cdot O_2$ above the Heisenberg ladder quartet state using CASSCF. The unpaired α spin density is shown as the blue surfaces and the unpaired β spin density is represented by the green surfaces. The states show the presence of unpaired spin density on oxygen and complex for the 2E state.

This agrees with experimental results on larger Cr(III) based complexes where the 2E state lifetime is significantly shortened by the presence of O_2 .^{9,16}

CONCLUSIONS:

Theoretical methods in this study supports the experimental observation of Cr(III) based catalysts being quenched by ground state O_2 molecules. The FD-DFT and NEVPT2 can produce excitation energies that are reasonable for this quenching process, and both can model the proper combination of determinants that represent the state. The CASSCF spin density plots help visualize the states involved and confirm that the 2E state is the likely state by which the chromium complexes are quenched. Also visualized is the complexity of the states involved and shortcomings of traditional DFT in modeling these states. Continued development is needed on modern DFT methods to produce techniques that can model complicated transition metal photocatalysts in a computational inexpensive manner.

REFERENCES

- (1) Cano-Yelo, H.; Deronzier, A. Photo-Oxidation of Some Carbinols by the Ru(II) Polypyridyl Complex-Aryl Diazonium Salt System. *Tetrahedron Lett.* **1984**, *25* (48), 5517–5520.
- (2) Meyer, T. J. Chemical Approaches to Artificial Photosynthesis. *Acc. Chem. Res.* **1989**, *22* (5), 163–170.
- (3) Yoon, T. P.; Ischay, M. A.; Du, J. Visible Light Photocatalysis as a Greener Approach to Photochemical Synthesis. *Nat. Chem.* **2010**, *2* (7), 527–532.
- (4) Narayanam, J. M. R.; Stephenson, C. R. J. Visible Light Photoredox Catalysis: Applications in Organic Synthesis. *Chem Soc Rev* **2011**, *40* (1), 102–113.
- (5) Tucker, J. W.; Stephenson, C. R. J. Shining Light on Photoredox Catalysis: Theory and Synthetic Applications. *J. Org. Chem.* **2012**, *77* (4), 1617–1622.
- (6) Xuan, J.; Xiao, W.-J. Visible-Light Photoredox Catalysis. *Angew. Chem. Int. Ed.* **2012**, *51* (28), 6828–6838.
- (7) Prier, C. K.; Rankic, D. A.; MacMillan, D. W. C. Visible Light Photoredox Catalysis with Transition Metal Complexes: Applications in Organic Synthesis. *Chem. Rev.* **2013**, *113* (7), 5322–5363.
- (8) Stevenson, S. M.; Shores, M. P.; Ferreira, E. M. Photooxidizing Chromium Catalysts for Promoting Radical Cation Cycloadditions. *Angew. Chem. Int. Ed.* **2015**, *54* (22), 6506–6510.
- (9) Higgins, R. F.; Fatur, S. M.; Shepard, S. G.; Stevenson, S. M.; Boston, D. J.; Ferreira, E. M.; Damrauer, N. H.; Rappé, A. K.; Shores, M. P. Uncovering the

- Roles of Oxygen in Cr(III) Photoredox Catalysis. *J. Am. Chem. Soc.* **2016**, *138* (16), 5451–5464.
- (10) Pfeil, A. Quenching of the Phosphorescence of Some Chromium(III) Complexes by Molecular Oxygen. *J. Am. Chem. Soc.* **1971**, *93* (21), 5395–5398.
- (11) Yang, Y.; Liu, Q.; Zhang, L.; Yu, H.; Dang, Z. Mechanistic Investigation on Oxygen-Mediated Photoredox Diels–Alder Reactions with Chromium Catalysts. *Organometallics* **2017**, *36* (3), 687–698.
- (12) Frisch, M. J.; Trucks, G. W.; Schlegel, H. B.; Scuseria, G. E.; Robb, M. A.; Cheeseman, J. R.; Scalmani, G.; Barone, V.; Mennucci, B.; Petersson, G. A.; et al. *Gaussian 09 Revision D.01*.
- (13) Neese, F. The ORCA Program System. *Wiley Interdiscip. Rev. Comput. Mol. Sci.* **2012**, *2* (1), 73–78.
- (14) Russo, T. V.; Martin, R. L.; Hay, P. J. Density Functional Calculations on First-Row Transition Metals. *J. Chem. Phys.* **1994**, *101* (9), 7729–7737.
- (15) Frisch, M. J.; Trucks, G. W.; Schlegel, H. B.; Scuseria, G. E.; Robb, M. A.; Cheeseman, J. R.; Scalmani, G.; Barone, V.; Petersson, G. A.; Nakatsuji, H.; et al. *Gaussian 16 Revision A.03*.
- (16) Serpone, N.; Jamieson, M. A.; Hofmann, M. Z. Oxygen Quenching of Metal-Centered Excited States of Polypyridyl Complexes of Chromium (III). *Inorganica Chim. Acta* **1978**, *31*, L447–L449.

CHAPTER 5: COMPARISON OF EXCITED STATE PROPERTIES OF CHROMIUM(III) AND VANADIUM(II) COMPLEXES: POTENTIAL AS PHOTOCATALYSTS¹

INTRODUCTION:

Across all chemical industries there is a push for more environmentally friendly and sustainable processes. Photocatalysis has become an attractive prospect for chemical transformations that conventionally rely on harsh reaction conditions and stoichiometric reagents generating waste. Many research groups have shown that photocatalysts can be used to mediate traditional synthetic reactions. Yoon et al. showed that visible light could actually be used as a reagent with a $\text{Ru}(\text{bpy})_3^{2+}$ photocatalyst for [2+2] cycloadditions.¹ However, this reaction as well as other successful phototransformations have relied on the use of metal catalysts made up of ruthenium and other rare metals such as rhenium and iridium which are not sustainable or economically viable in large scale application.²

There is a need for a more earth abundant alternative to these rare metals. First row transition metals are several orders of magnitude more abundant than rare metals. There is potential for first row transition metal photocatalysts. Stevenson et al. showed that a chromium(III) complex was capable of photooxidizing catalyzed Diels-Alder cycloadditions. It is theorized that rare metal complexes can be substituted by earth

¹ The work in this chapter was done by Jacob M. Nite and Collette M. Nite. Jacob M. Nite calculated the vibrational distortion plots, including the structure alignments for the chromium and vanadium complexes.. He also calculated the PDO distortion pathways for chromium and vanadium as well as performed the SORCI calculations including the generation of the potential energy curve plots. Collette M. Nite performed the geometric optimization calculations for all complexes with in the chapter. She also performed all TDDFT excited state calculations and generated all absorption spectra. Both authors contributed equally to the text of the chapter.

abundant first row transition metal complexes for phototransformations on a much broader scale. However, pursuit of this goal requires in depth theoretical and experimental research, as first row transition metal complexes behave differently than second and third row transition metal complexes.

First row transition metal complexes are much more labile than second and third row metals, yielding much more reactive and less stable catalysts. In addition, first row metals are electron spin active, resulting in wildly different chemistry with complicated excited state manifolds and thus difficult characterizations. There is much more interplay between first row transition metals and their ligands, requiring a higher degree of care in their complex design than second and third row counterparts.

The choice of ligand is therefore very important when designing these catalysts. Ligands are often noninnocent and can have a drastic effect on the photoabsorption of a complex. Ligands often dictate the spin state of a metal in a given complex, determining if the complex will be high- or low-spin. Substitution of a different metal in the same ligand can yield very different results, because metals interact differently with ligands. The differences between metal-swapped complexes can be more abrupt than changes to the ligands due to the limited metal center candidates combined with the substantial difference in properties of the metal centers. Compared to an enormous range of ligand design choices, the handful of metals in the first-row dictate that careful selection of the proper metal is crucial.

In this paper we focus on vanadium and its potential for photocatalysis. V(II) is of d^3 electronic configuration, just as Cr(III). While Cr(III) has beneficial properties such as long excited state lifetimes and demonstrable photocatalytic ability, it is not the most

desirable metal for environmental concerns. V(II) is not readily oxidizable into carcinogenic species. Comparing the photophysical and photochemical between V(II) and Cr(III) may lead to insight on how the properties of the ligand dictate the total complex properties when electronic configuration is held constant. In this paper we use theoretical methods in order to compare Cr(III) and V(II) complexes on the basis of their photophysical and photochemical properties in order to elucidate their differences and vanadium's potential as a photocatalyst.

THEORETICAL METHODS:

The complexes studied were comprised of the V(II), Cr(III), Mn(II), Fe(III), Co(III), and Zn(II) metal centers paired with several ligands: a Schiff base tripodal ligand with a bridgehead nitrogen, a salen derivative, bipyridine, and 1,3-propanedionato(PDO).

STRUCTURE OPTIMIZATION AND THEORETICAL SPECTRA:

The structures of each complex were optimized using DFT with the APF-D functional and the 6-311+G* basis set. The time-dependent density functional theory (TDDFT) excited states were calculated for the first 24 excited states of each complex to insure all relevant excited states were included. Convoluting each TDDFT transition with a Gaussian line shape with a linewidth of 0.093 eV at the full-width half-maximum, theoretical absorption spectra were plotted. The linewidth was chosen to approximate average excited state linewidths. The lowest excited doublet state was obtained by broken-symmetry DFT. The spin density plots were calculated using Gausview using a course grain cube and an isovalue of 0.003 to insure optimal visualization of the differences between the chromium and vanadium complexes. All DFT calculations were computed using the Gaussian 09d software suite.³

Cr / V(PDO)₃:

Additionally, the complexes with the ligand 1,3-propanedionato (PDO) were studied to gain an insight into the excited state behavior of Cr(III) and V(II). The electronic states are references to an O_h point group to remain consistent with the literature.⁴ The $^4A_{2g}$ ground states of Cr(III)PDO₃ and V(II)PDO₃ were optimized using the same DFT approaches used above. The lowest excited state structures of the Cr(III) and V(II) complexes were calculated corresponding to the Jahn-Teller distorted $^4T_{2g}$ state constrained to the C_2 symmetry point group. These structures are analogous to the Cr(III)(AcAc)₃ $^4T_{2g}$ cited previously in literature.⁴ We aligned the ground state and excited state structures to form a linear pathway in the form of Miller et al. and formed linearly interpolated structures along path.⁵

The excited states of each structure along the distortion coordinate were calculated using the spectroscopy oriented configuration interaction (SORCI) method to construct the excited state pathways between the ground state and relaxed excited state. The initial wave function for each structure was calculated using the B3LYP functional with a cc-(p)VDZ basis set for all atoms except the metal center which used a cc-pCVTZ basis set. Each wave function was refined using a complete active space self-consistent field wave function (CASSCF) with a 3,5 active space and state averaging. All SORCI calculations utilizing the CASSCF wave functions were done including additional core electrons beyond the CASSCF active space. The B3LYP DFT, CASSCF, and SORCI calculations were computed using the ORCA 3.0.3 electronic structure suite.⁶

VIBRATIONAL PROJECTIONS:

The vibrational contributions to the difference between the ground state and excited states of Cr(III)bpy₃ and V(II)bpy₃ were calculated using a vibrational mode projection scheme used by Ando et al.⁴ Briefly, the vibrational normal modes of both Cr(III)bpy₃ and V(II)bpy₃ were calculated for the ground state geometry. The excited state structure was aligned to the ground state structure using the same criteria used for the linear reaction pathway in the SORCI calculations where any translational and angular momentum were removed from the structure. The excited state center of mass was translated to the center of mass of the ground state and the excited state structure was rotated by the Euler indices that satisfy the equation

$$\sum_i m_i (\vec{R}_i^r \times \vec{R}_i^p) = 0 \quad (0.1)$$

where i is over all atoms, m_i is the mass of atom i , and \vec{R}_i is the Cartesian coordinates of atom i .⁵ The resulting structures were examined to ensure that the alignment did not contain any unphysical atom movements between the structures. This ensures that no vibrational modes are projected onto differential distortions due to translations or rotations of the whole complex.

The frequency calculation of the ground state includes the eigenvalues and eigenvectors of the diagonalized Hessian, which describe the vibrational energies and mode motion in terms of atom displacements, \mathbf{L}_{gs} . A Duschinsky vector, \mathbf{K}_{gs} , is calculated using the formula

$$\mathbf{K}_{gs} = \mathbf{M} \mathbf{L}_{gs} \mathbf{R}_d \quad (0.2)$$

where \mathbf{M} is a matrix containing the masses of each atom and, \mathbf{R}_d is the difference vector of atomic coordinates between the ground and excited states.⁴ This results in a

vector, \mathbf{K}_{gs} , that describes a relative amount of each vibrational mode resulting from the distortion between the ground and excited states.

RESULTS & DISCUSSION:

TDDFT:

When first analyzing potential ligand frameworks for photocatalysis, the focus was first on Schiff base moieties, a class of ligands containing a nitrogen-carbon double bond with the nitrogen bonded to an alkyl or aryl group. These ligands were known for straightforward syntheses with the ability to stabilize many different metals. The structure of the Schiff base moiety and the theoretical absorption spectra of the Schiff base ligand complexed various first row transition metals are shown in Figure 5.1. What was particularly intriguing when comparing the spectra of varying metals was the unique spectral feature of the V(II) complex (in purple) at around 630 nm. No other metal exhibited a broad intense peak at the low energy visible region.

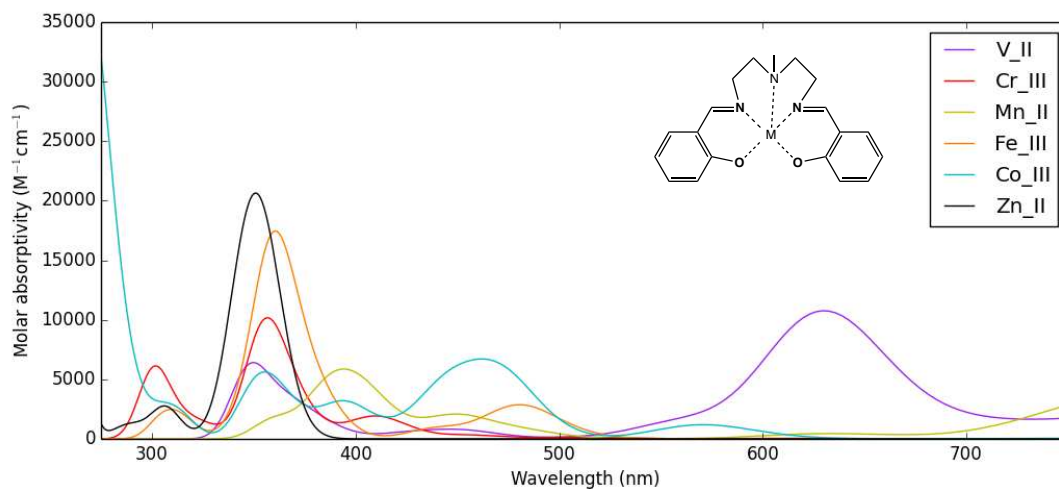


Figure 5.1: TDDFT(APF-D/6-311+G*) spectra of various first row transition metal Schiff base complexes.

Spectra of complexes of the salen Schiff base-derived ligand were also computed and analyzed for photochemical properties. The salen ligand is known for its

two imine nitrogens and two oxygen atoms complexed to the metal center. In Figure 5.2, a structural derivative was analyzed with amido groups substituted for the oxygen atoms. The theoretical spectra of the given complex with different first row metals are in Figure 5.2.

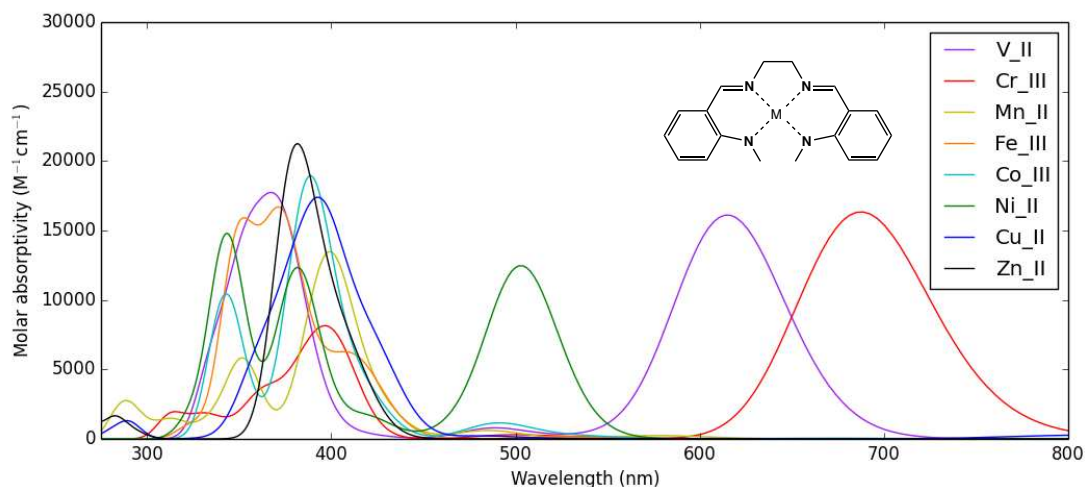


Figure 5.2: TDDFT(APF-D/6-311+G*) spectra of various first row transition metal salen type complexes.

Again, the V(II) salen derivative complex (in purple) had intense absorption in the low energy visible region marked by a broad peak centered around 610 nm. Notable also is the almost identical broad structural feature of the Cr(III) salen complex (in red), which is red shifted from the V(II) complex centered at around 690 nm. This spectrum led to the promising hypothesis that a d^3 V(II) metal complex could have similar photochemical properties as a d^3 Cr(III) metal complex, and therefore vanadium could be exploited as an alternative photocatalyst.

SPIN DENSITY PLOTS:

Electronic structure calculations were then used to explore potential differences between Cr(III) and V(II) complexes. Spin density shows where the unpaired spin electron is with respect to the metal and ligand of the complex. Spin density plots for a

few Cr(III) and V(II) complexes for their ground quartet states (left column) and their excited doublet states (right column) are shown in Table 5.1, Table 5.2, and Table 5.3.

Looking at the Cr(III)trisbipyridine case, the quartet state is immediately evident as the three unpaired alpha spin electrons are represented by the blue (alpha spin) cubic structure centered on the Cr(III) metal. In the doublet case, there is nodal beta spin character (represented in green) now on the metal where there is now one unpaired spin. Similar behavior can be described for the V(II) d^3 metal, where the spin density on the metal looks very similar to the Cr(III) case. However, a notable difference is the presence of spin density out on the bipyridine ligands in both the quartet and the doublet cases for vanadium. The importance of this density on the V(II) complex is related to the decreased quartet-doublet energy difference for the V(II) complex compared to the Cr(III) complex (1.08 eV versus 1.62 eV). The beta electron density on the ligand and energy differences suggests that the doublet state is more stable for the V(II) complex compared to the Cr(III) analog, decreasing the available chemical potential to catalyze reactions.

Another common photocomplex structure, the podand ligand complex, was compared. For the Cr(III) case there was again similar quartet and doublet behavior on the metal, with most spin density centered around the metal. In the V(II)pod complex doublet case, a large portion of the unpaired spin is again pushed out far onto the ligand structure.

Ester groups were added to the pod ligand structure in order to try inhibit the ligand from containing significant amounts of unpaired spin density. The trend still held

Table 5.1: Spin density plots of quartet and doublet states of the Cr(III)bpy₃ and V(II)bpy₃ photocomplexes.

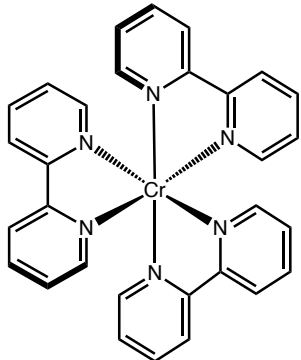
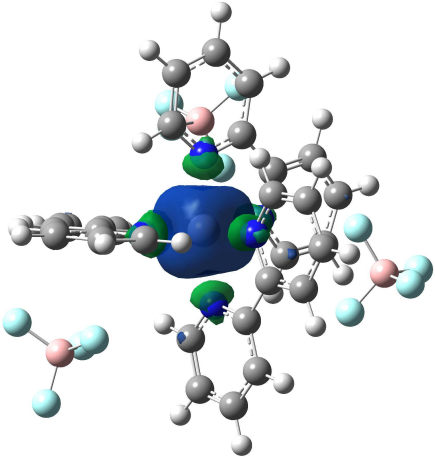
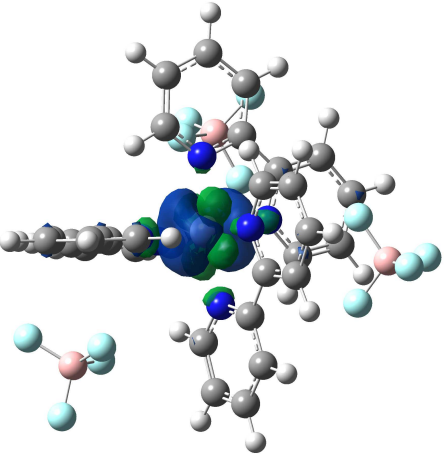
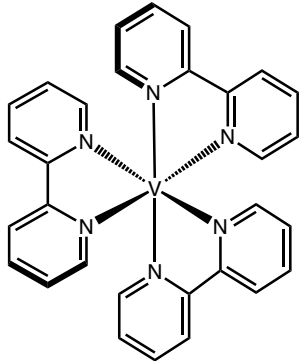
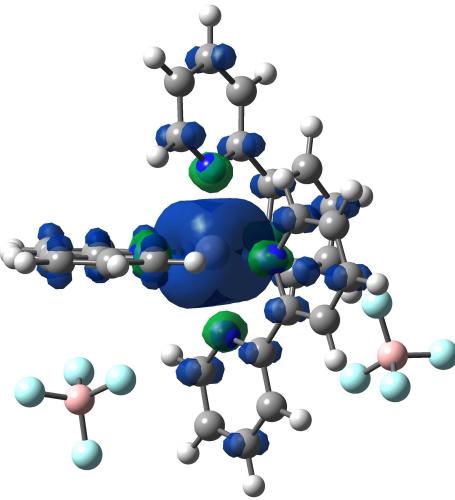
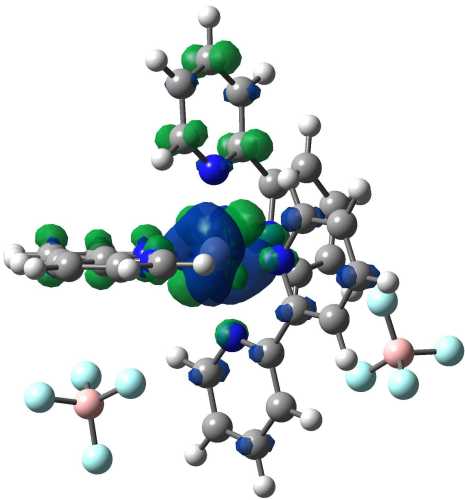
	Quartet	Doublet
<p>Cr(III)bpy₃</p> 		
<p>V(II)bpy₃</p> 		

Table 5.2: Spin density plots of quartet and doublet states of the Cr(III)pod and V(II)pod photocomplexes.

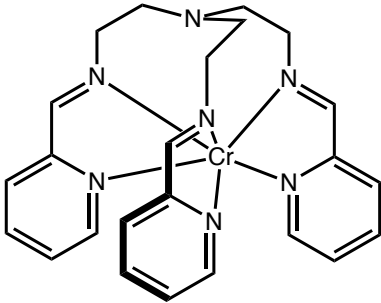
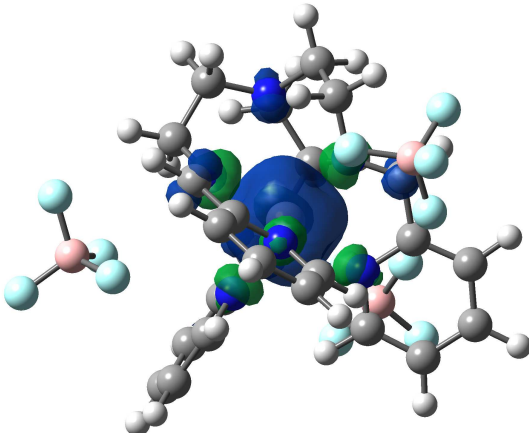
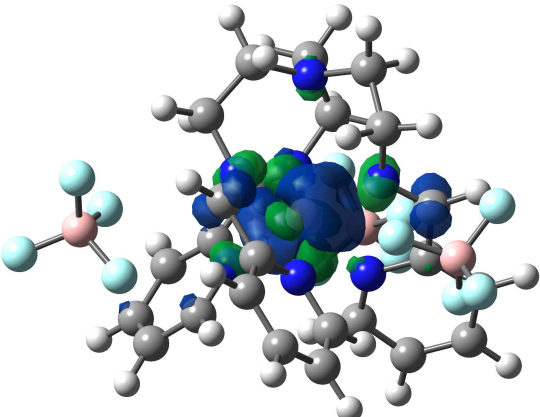
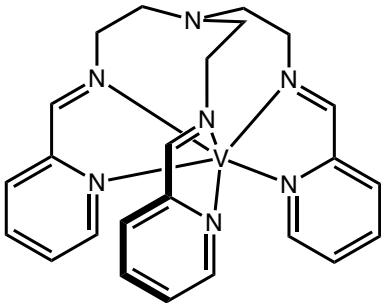
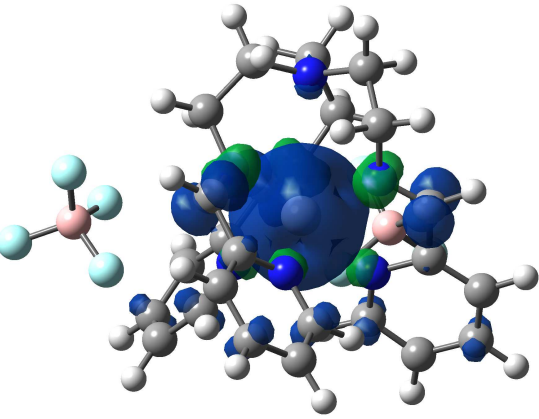
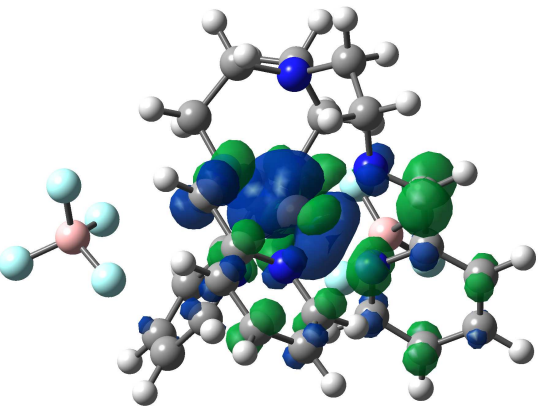
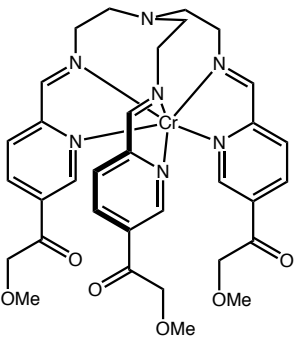
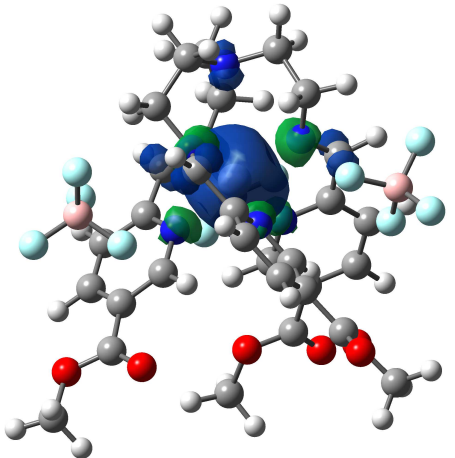
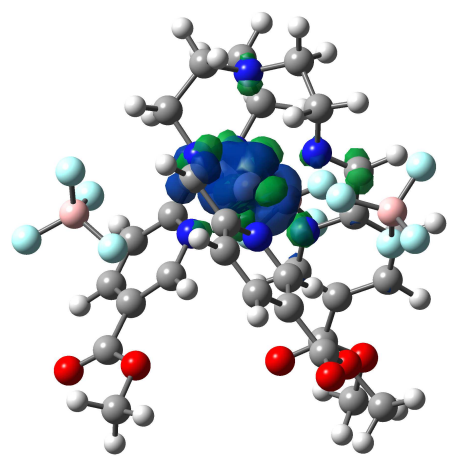
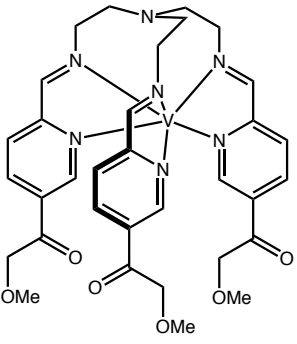
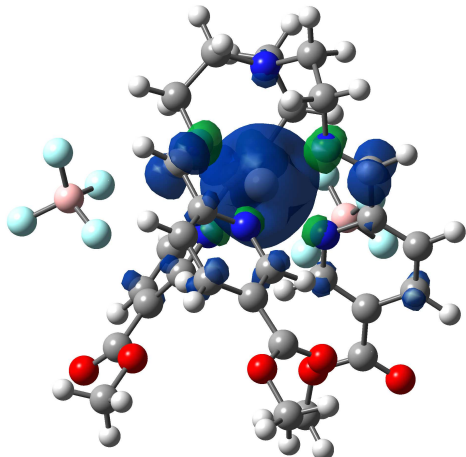
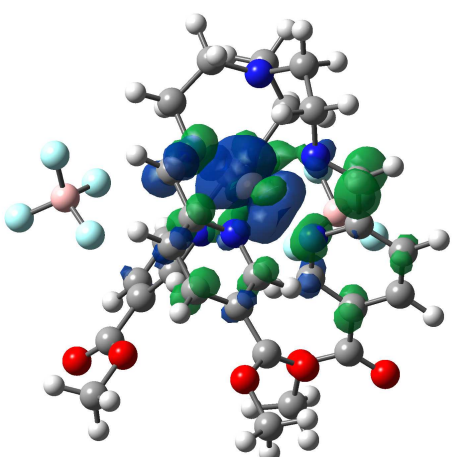
	Quartet	Doublet
<p>Cr(III)pod</p> 		
<p>V(II)pod</p> 		

Table 5.3: Spin density plots of quartet and doublet states of the Cr(III)esterpod and V(II)esterpod photocomplexes.

	Quartet	Doublet
<p>Cr(III)esterpod</p>  <p>The chemical structure shows a central Chromium (Cr) atom coordinated to a terpyridine-like ligand and three methoxycarbonyl groups. The ligand consists of three pyridine rings connected at their 2-positions, with a central nitrogen atom in a macrocyclic ring.</p>	 <p>3D spin density plot for the quartet state of Cr(III)esterpod. The central Cr atom is shown as a large blue sphere. Spin density is distributed across the ligand, with significant positive (blue) and negative (green) contributions on the nitrogen and carbon atoms of the pyridine rings.</p>	 <p>3D spin density plot for the doublet state of Cr(III)esterpod. The central Cr atom is shown as a large blue sphere. The spin density distribution is similar to the quartet state but with a different overall magnitude and distribution pattern.</p>
<p>V(II)esterpod</p>  <p>The chemical structure shows a central Vanadium (V) atom coordinated to a terpyridine-like ligand and three methoxycarbonyl groups, identical to the Cr(III)esterpod complex.</p>	 <p>3D spin density plot for the quartet state of V(II)esterpod. The central V atom is shown as a large blue sphere. The spin density distribution is similar to the Cr(III)esterpod quartet state.</p>	 <p>3D spin density plot for the doublet state of V(II)esterpod. The central V atom is shown as a large blue sphere. The spin density distribution is similar to the Cr(III)esterpod doublet state.</p>

with Cr(III) complex keeping much electron density centered on the metal while the spin density of the V(II) complex was again displaced out onto the ligand.

As evident from these spin density plots, there is a strong difference where the lone electron is going following excitation to the doublet state in the Cr(III) and V(II) case. In the V(II) case there is significant delocalization of the quartet spin on the ligand as well as the doublet state with antiparallel spin. In fact, increasing donating ligands by methyl substituting the pyridine ligands didn't make much of a difference. There seems to be favorable exchange for the quartet state, but in the case of the doublet state for V(II), the α and β electrons want to be delocalized as much as possible. The d orbitals on the vanadium metal are much larger than the d orbitals of the chromium metal due to d orbital expansion. Therefore this delocalization decreases the magnitude of excitation for the vanadium complexes, which greatly hinders its potential as a prominent photocatalyst.

VIBRATIONAL PROJECTION SPECTRA:

The vibrational distortion projection plots highlight additional differences between the Cr(III) and V(III) complexes by comparing the vibrational normal mode components that make up the distortion from the ground state to the excited state. Comparing the plots for Cr(III)(bpy)₃ and V(II)(bpy)₃ shows a two to six times larger dependence on very low modes less than 100 cm⁻¹ for the V(II) complex compared the Cr(III) complex (See Figure 5.3). For V(II)(bpy)₃, the dominant modes are those that consist of symmetric ligand wags, symmetric torsions between the pyridines, and symmetric ligand stretches with the metal center. Many of the Cr(III)(bpy)₃ dominant modes are shared with V(II)(bpy)₃ such as the symmetric ligand wags and stretches, but also

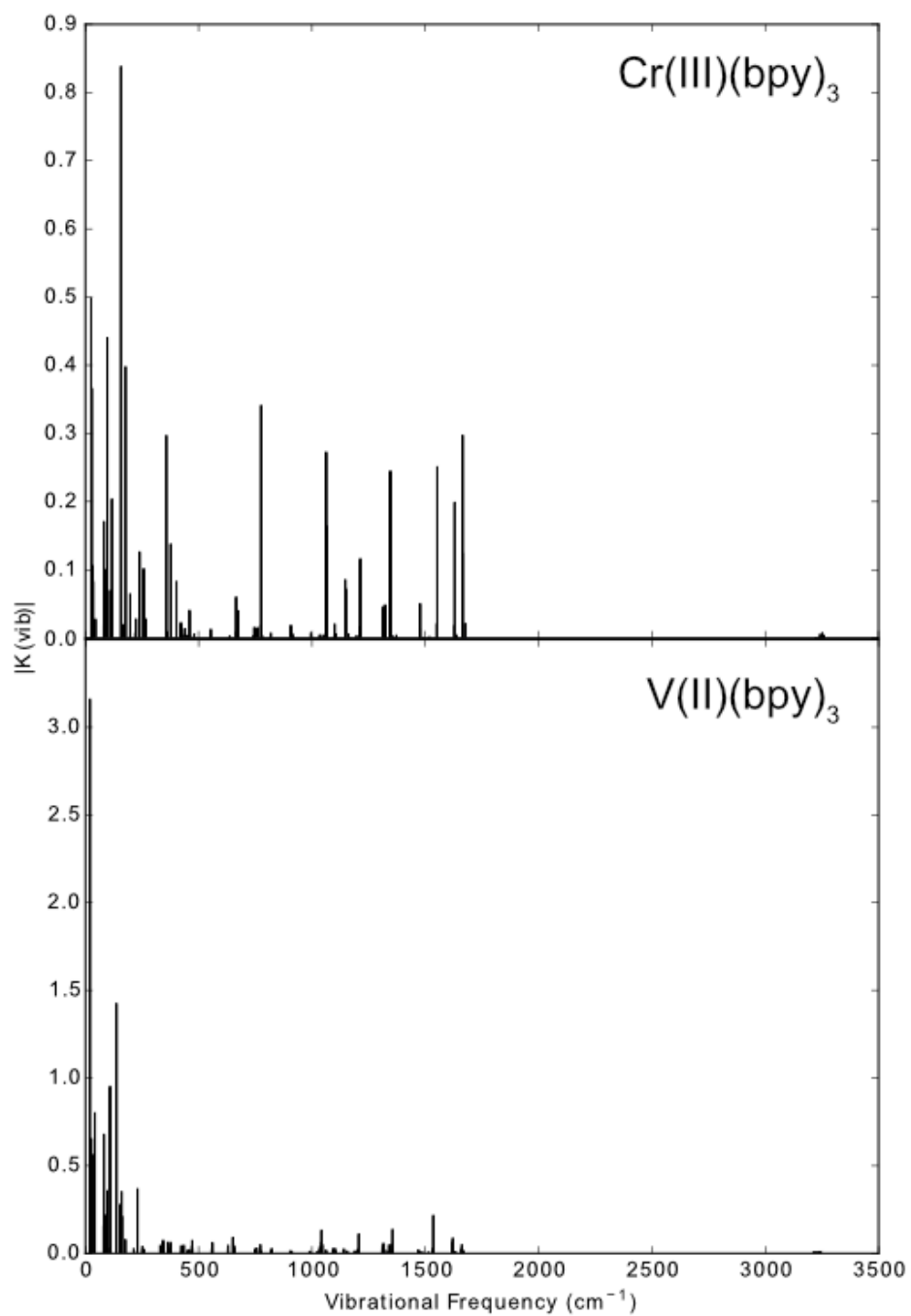


Figure 5.3: Vibrational distortion projection plot between the ground state and excited state quartet structures for Cr(III)(bpy)₃ and V(II)(bpy)₃. The units of the K elements are in Å amu^{1/2}.

includes an asymmetric pyridine torsion, asymmetric ligand wag, and an asymmetric ligand-metal center stretch. In addition, an intraligand stretch on a single ligand is also a dominant mode. This implies that not only are the excited state structures different between the two metal center based ligands, the excited state pathway that the complex takes upon excitation is very different. Whether the different pathways lead to an intersystem crossing event requires additional measurements to determine. However, these results suggest that Cr and V isoelectronic complexes with identical ligands cannot be assumed to behave similar in their excited states.

SORCI:

The excited state potential energy surfaces of the PDO ligand complexes for Cr(III) and V(II) provide additional insight into the differences between the two metals within similar complexes. The Cr(III)(AcAc)₃ complex has been widely studied in literature. The complex ground state is ⁴A_{2g}. Upon initial excitation, the complex is promoted to the ⁴T_{2g} state. The complex rapidly relaxes to the ²E_g, a long-lived state that is thought to be primary state through which the complex performs catalytic functions.

Plotting the excited states of each state along the linear path between the ⁴T_{2g} and ²E_g excited states, an immediate difference is seen between the Cr(III)(PDO)₃ and the V(II)(PDO)₃ complexes, see Figure 5.4. For the Cr(III) complex, a prominent feature of the plot is the crossing of the lowest excited quartet states with the lowest doublets around R = 0.67 along the distortion coordinate. This provides a low barrier pathway to the ²E_g state since the states in the crossing region do exhibit mixed doublet/quartet character when spin-orbit coupling contributions are included in the calculation. This

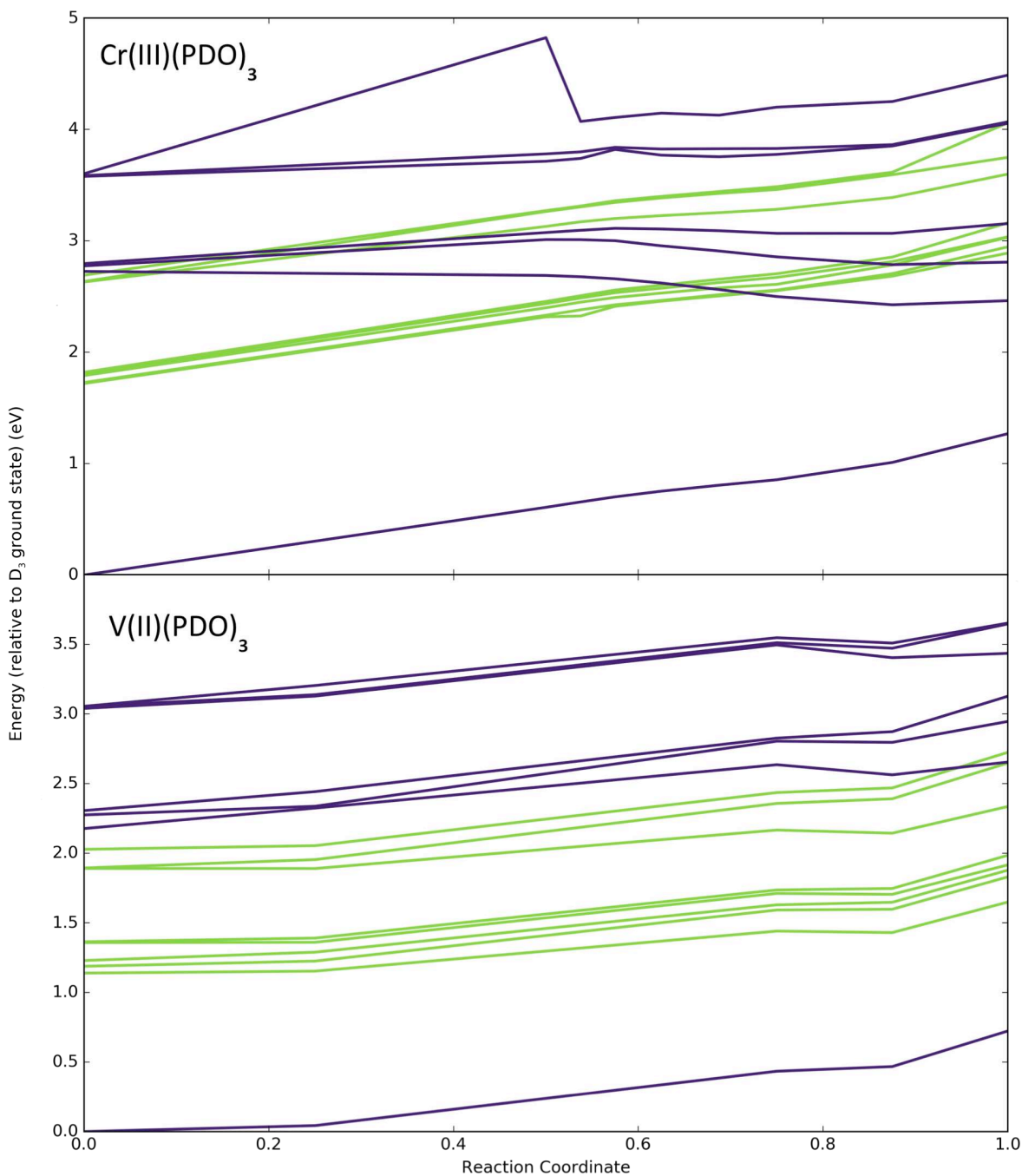


Figure 5.4: Plot of excited state energies of $X(\text{PDO})_3$ complexes where X is Cr(III) or V(II) along a linear distortion reaction coordinate between the ${}^4A_{2g}$ and ${}^2T_{2g}$ optimized geometries. The purple lines represent the quartet states and the green lines represent the doublet states. The V(II) and Cr(III) complexes show strikingly different behavior along the distortion coordinates, where the Cr(III) complex shows a complete crossing several doublet and quartet states while the V(II) complex shows minimal places where the states are degenerate.

agrees with experimental results demonstrating the fast intersystem crossing to the 2E_g state in Cr(III)(AcAc)_3 .

The excited states along the distortion coordinate show a different trend for the V(II)(PDO)_3 complex. The lowest excited quartets rise in energy with the doublets as the structure distorts towards the stable ${}^4T_{2g}$ state. This contrasts the Cr(III) complex where the lowest excited quartets decrease in energy as a function of distortion. This causes no crossings between the excited quartets and doublets in the V(II) complex. While the difference between these two excited state pathways is not definitive proof that V(II)(PDO)_3 is unable to reach the 2E_g state, it does suggest that V(II) complexes may be significantly less likely to reach a stable doublet state upon excitation compared to a Cr(III) analog. Without a complete map of the potential energy surface, it is not known whether other low barrier quartet to doublet transitions exist, but the most direct path does not contain one.

CONCLUSIONS:

We have highlighted the substantial differences exhibited by various transition metal complexes with Cr(III) and V(II) with respect to their excited states. The absorption spectra demonstrate the wide range of excited states that are populated upon vertical absorption, which can lead to shifts of more than 100 nm in the visible range. This is a very useful property to try to exploit to obtain catalysts that absorb in a desired range. However, the change in absorption also implies a change to excited state dynamics as well. The spin density plots, vibrational distortion plots, and SORCI derived excited state potential energy curves demonstrate a significant change to the excited state dynamics from the substitution of Cr(III) with V(II) . Having a complex with

desirable excited state properties is critical to a photocatalyst's ability to participate in redox chemistry. Evidence demonstrating that V(II) based photocatalysts do not easily form a long-lived excited state through intersystem crossing reduces their utility as photocatalysts.

REFERENCES

- (1) Yoon, T. P.; Ischay, M. A.; Du, J. *Nat. Chem.* **2010**, 2 (7), 527–532.
- (2) Tucker, J. W.; Stephenson, C. R. J. *J. Org. Chem.* **2012**, 77 (4), 1617–1622.
- (3) Frisch, M. J.; Trucks, G. W.; Schlegel, H. B.; Scuseria, G. E.; Robb, M. A.; Cheeseman, J. R.; Scalmani, G.; Barone, V.; Mennucci, B.; Petersson, G. A.; Nakatsuji, H.; Caricato, M.; Li, X.; Hratchian, H. P.; Izmaylov, A. F.; Bloino, J.; Zheng, G.; Sonnenberg, J. L.; Hada, M.; Ehara, M.; Toyota, K.; Fukuda, R.; Hasegawa, J.; Ishida, M.; Nakajima, T.; Honda, Y.; Kitao, O.; Nakai, H.; Vreven, T.; Montgomery, Jr., J. A.; Peralta, J. E.; Ogliaro, F.; Bearpark, M.; Heyd, J. J.; Brothers, E.; Kudin, K. N.; Staroverov, V. N.; Kobayashi, R.; Normand, J.; Raghavachari, K.; Rendell, A.; Burant, J. C.; Iyengar, S. S.; Tomasi, J.; Cossi, M.; Rega, N.; Millam, J. M.; Klene, M.; Knox, J. E.; Cross, J. B.; Bakken, V.; Adamo, C.; Jaramillo, J.; Gomperts, R.; Stratmann, R. E.; Yazyev, O.; Austin, A. J.; Cammi, R.; Pomelli, C.; Ochterski, J. W.; Martin, R. L.; Morokuma, K.; Zakrzewski, V. G.; Voth, G. A.; Salvador, P.; Dannenberg, J. J.; Dapprich, S.; Daniels, A. D.; Farkas, Ö.; Foresman, J. B.; Ortiz, J. V.; Cioslowski, J.; Fox, D. J. *Gaussian 09 Revision D.01*.
- (4) Ando, H.; Iuchi, S.; Sato, H. *Chem. Phys. Lett.* **2012**, 535, 177–181.
- (5) Miller, W. H.; Ruf, B. A.; Chang, Y.-T. *J. Chem. Phys.* **1988**, 89 (10), 6298–6304.
- (6) Neese, F. *Wiley Interdiscip. Rev. Comput. Mol. Sci.* **2012**, 2 (1), 73–78.

CHAPTER 6: FUTURE DIRECTIONS

This work presented shows the formalism of FD-DFT as well as its applications and utility in studying first-row transition metal photocatalysts. In its current state, it has shown promise as being a useful method for the calculation of excited state multiplets, which are common in long-lived excited states in transition-metal complexes, with low computational cost. However, while the foundational work on FD-DFT has been established, many further improvements are envisioned which would improve the stability, applicable molecular system excited states, non-energetic calculations.

In its current iteration, FD-DFT can successfully converge to a stable wave function through an SCF procedure using a GVB wave function for relatively simple systems. Large systems that represent photocatalysts in synthetic applications are not stable under SCF iterations. One hindrance towards SCF stability is the GVB wave function itself, which is not as efficient as a single effective Hamiltonian with a direct inversion in the iterative subspace (DIIS) optimizer. Since the FD-DFT equations do not depend on the GVB formalism, an implementation in another wave function type may help convergence. In addition, the functionals themselves do not display even SCF convergence speed among test cases. The functionals used in this work were chosen to represent common and recent functionals in literature. Functionals designed to work with the finite difference approach in this dissertation could improve SCF convergence as well as excitation energies.

FD-DFT is currently only rigorously implemented for excited state multiplets. The initial states of interest for the chromium catalysts could be described adequately by

multiplet states. However, closed shell pairs are of interest as well. For example, the second degenerate ${}^1\Delta$ and the ${}^1\Sigma^+$ states of O_2 are comprised of two orbitals in a closed shell pair. The addition of pairs is well described in the GVB-PP formalism, and FD-DFT can be used for these wave functions. The ${}^1\Delta$ and the ${}^1\Sigma^+$ states of O_2 do converge to their proper states if the a_{ij} and b_{ij} coefficients are given, but the current limitation is the lack of an iteration scheme to solve for optimal a and b coefficients. Small modifications to the current perfect pair solving scheme would be sufficient to allow for the inclusion of perfect pairs in a FD-DFT wave function.

The final large improvement to the FD-DFT method would be the addition of analytical gradients to the converged FD-DFT wave function. The addition of the gradient to the FD-DFT calculation would allow for post SCF calculations such as geometric optimizations based on excited states. As seen with $Cr(III)(AcAc)_3$ -like systems, geometric distortions are a key component of understanding the excited states of transition metal complexes. Analytical gradients are particularly desirable due to the increase in computation speed over numerical gradients. Fortunately, GVB wave functions as well as DFT potentials both have well-defined analytical gradient methods implemented in modern electronic structure codes. Use of the same FD-DFT equations should yield expressions to obtain analytical gradients for any FD-DFT wave function.

APPENDIX A: BROKEN SYMMETRY WAVEFUNCTIONS

Since the 1970s the energies of single determinant descriptions of different M_s states have been combined to provide estimates of the DFT energies of spin-restricted open shell systems. Approaches that have been commonly used are the broken symmetry spin-projected (BS S-P) approaches, which are formulated in terms of a Heisenberg spin Hamiltonian, Eq. (A.1) or the sum rules (SR) methodology of Ziegler, Rauk, and Baerends.¹

$$E = -2J\vec{S}_a \cdot \vec{S}_b \quad (\text{A.1})$$

The Noodleman and Davidson broken symmetry spin-projection approach for obtaining J is described in Eq. (A.2) where E_{HS} and E_{BS} are the total energies for the high spin and lowest M_s wave functions, and S_{max} is for the high spin wavefunction.²

$$J = -\frac{E_{\text{HS}} - E_{\text{BS}}}{S_{\text{max}}^2} \quad (\text{A.2})$$

An alternative, the approximate spin projection (AP) from Yamaguchi, incorporates S^2 for the broken symmetry state as given in Eq. (A.3).³

$$J = \frac{E_{\text{HS}} - E_{\text{BS}}}{\langle S^2 \rangle_{\text{HS}} - \langle S^2 \rangle_{\text{BS}}} \quad (\text{A.3})$$

While these approaches provide an estimate of the energies for proper spin eigenfunctions, neither provides a variational treatment of the wavefunction. In the BS S-P approach the energies of a high-spin determinant and a single lowest-spin determinant are computed and used to provide an estimate for the proper lowest spin energy.

For three-electron doublets there are three distinct $M_s = 1/2$ determinants which, for non-symmetry constrained systems, may differ in energy. These three determinants

need to be combined into two orthogonal doublets. For both the BS S-P approach and the SR methodology, there is no guarantee that the individual determinant models are orthogonal, nor is there a mechanism for treating the coupling between spin eigenfunctions. Frank, Hutter, Marx, and Parrinello have reported a spin-restricted open shell singlet treatment wherein they constructed the Fock matrices from a linear combination of high-spin and broken symmetry energy expressions.⁴

For the strongly correlated/weakly interacting systems of interest where antiferromagnetic coupling may dominate and more than two electrons are involved, a perfect pairing description is not adequate, nor is a description involving orthogonal singly occupied orbitals. Since the 1970s, broken symmetry descriptions have been used for antiferromagnetically coupled systems since α and β are not required to be spatially orthogonal in a spin unrestricted wavefunction.⁵

Starting in the early 1980s Noodleman popularized the use of a broken symmetry unrestricted Kohn-Sham (UKS) wave function to compute magnetic interactions between weakly coupled electrons.² This model was demonstrated to serve as a computationally viable approximation to the proper many configuration wave function for magnetic systems. The model has also proven useful for describing bond breaking processes. Here the model is summarized for a two-electron system.

Consider bonding ϕ_b and antibonding ϕ_a molecular orbitals. In the context of multiplets, the triplet which places one electron each in ϕ_b and ϕ_a has been considered the ground state. For a discussion of broken symmetry models, used by DFT for multiplet systems as described in Chapter II as well as for antiferromagnetically coupled

systems, we consider the four possible two-electron configurations, see Eq. (A.4) to (A.7).

$$\psi_{S_1} = \phi_b \phi_b (\alpha\beta - \beta\alpha) \quad (\text{A.4})$$

$$\psi_T = (\phi_b \phi_a - \phi_a \phi_b) \left\{ \begin{array}{c} \alpha\alpha \\ \alpha\beta + \beta\alpha \\ \beta\beta \end{array} \right\} \quad (\text{A.5})$$

$$\psi_{S_2} = (\phi_b \phi_a + \phi_a \phi_b) (\alpha\beta - \beta\alpha) \quad (\text{A.6})$$

$$\psi_{S_3} = \phi_a \phi_a (\alpha\beta - \beta\alpha) \quad (\text{A.7})$$

The two molecular orbitals, ϕ_b and ϕ_a , and four states, Eq. (A.4)-(A.7), can be written in terms of non-orthogonal atomic spatial orbitals ϕ_l and ϕ_r , placed on left and right centers respectively, see Eq. (A.8).

$$\begin{aligned} \phi_b &= \frac{\phi_l + \phi_r}{\sqrt{2 + 2S_{lr}^2}} \\ \phi_a &= \frac{\phi_l - \phi_r}{\sqrt{2 - 2S_{lr}^2}} \end{aligned} \quad (\text{A.8})$$

Substitution of the representations in Eq. (A.8) into Eq. (A.4)-(A.7) provides localized orbital descriptions of these four states, see Eq. (A.9)-(A.12).

$$\psi_{S_1} = (\phi_l \phi_l + \phi_l \phi_r + \phi_r \phi_l + \phi_r \phi_r) (\alpha\beta - \beta\alpha) \quad (\text{A.9})$$

$$\psi_T = (\phi_l \phi_r - \phi_r \phi_l) \left\{ \begin{array}{c} \alpha\alpha \\ \alpha\beta + \beta\alpha \\ \beta\beta \end{array} \right\} \quad (\text{A.10})$$

$$\psi_{S_2} = (\phi_l \phi_l - \phi_r \phi_r) (\alpha\beta - \beta\alpha) \quad (\text{A.11})$$

$$\psi_{S_3} = (\phi_l \phi_l - \phi_l \phi_r - \phi_r \phi_l + \phi_r \phi_r) (\alpha\beta - \beta\alpha) \quad (\text{A.12})$$

Configurations ψ_{S_1} and ψ_{S_3} are of the same symmetry and hence can interact to lower the energy of the system. In a GVB representation the wave function is taken as the variational linear combination, see Eq. (A.13)

$$\psi = c_1^2 \psi_{S_1} - c_2^2 \psi_{S_3} \quad (\text{A.13})$$

In the limit of weak overlap yield, the simple minus combination prevails and the two-configuration molecular orbital description collapses to a simple valence bond description, see Eq. (A.14).

$$\psi_{S_1} - \psi_{S_3} = (\phi_l \phi_r + \phi_r \phi_l)(\alpha\beta - \beta\alpha) \quad (\text{A.14})$$

This wave function and the $M_s = 0$ triplet component, Eq. (A.10), are quite similar and can be expanded into spin orbitals, see Eq. (A.15) and (A.16), and then combined, Eq. (A.17) and (A.18).

$$\psi_{S_1} - \psi_{S_3} = \phi_l \phi_r \alpha\beta - \phi_l \phi_r \beta\alpha + \phi_r \phi_l \alpha\beta - \phi_r \phi_l \beta\alpha \quad (\text{A.15})$$

$$\psi_T = \phi_l \phi_r \alpha\beta + \phi_l \phi_r \beta\alpha - \phi_r \phi_l \alpha\beta - \phi_r \phi_l \beta\alpha \quad (\text{A.16})$$

$$\psi_{S_1} - \psi_{S_3} + \psi_T = \phi_l \phi_r \alpha\beta - \phi_r \phi_l \beta\alpha = A \phi_l \phi_r \alpha\beta \quad (\text{A.17})$$

$$\psi_{S_1} - \psi_{S_3} - \psi_T = \phi_r \phi_l \alpha\beta - \phi_l \phi_r \beta\alpha = A \phi_r \phi_l \alpha\beta \quad (\text{A.18})$$

The resulting localized wave functions, Eq. (A.17) and (A.18) place one spin on the left and one on the right yielding molecular orbitals that individually do not possess the symmetry of the molecule, hence the term broken symmetry. Further, while they are both $M_s = 0$ states, they are not eigenfunctions of S^2 , but rather spin-unrestricted wave functions. As ϕ_l and ϕ_r delocalize onto the alternate center (as a function of distance or overlap) the original ψ_{S_1} is recovered.

Energies, relative to two hydrogen atoms, of the various two electron wave function models of H_2 are collected in Figure A.1. The energy of the two-configuration or GVB model rises as R_{HH} increases, dissociating properly to two hydrogen atoms. The overlap between the non-orthogonal orbitals of the GVB pair, Eq. (A.19),

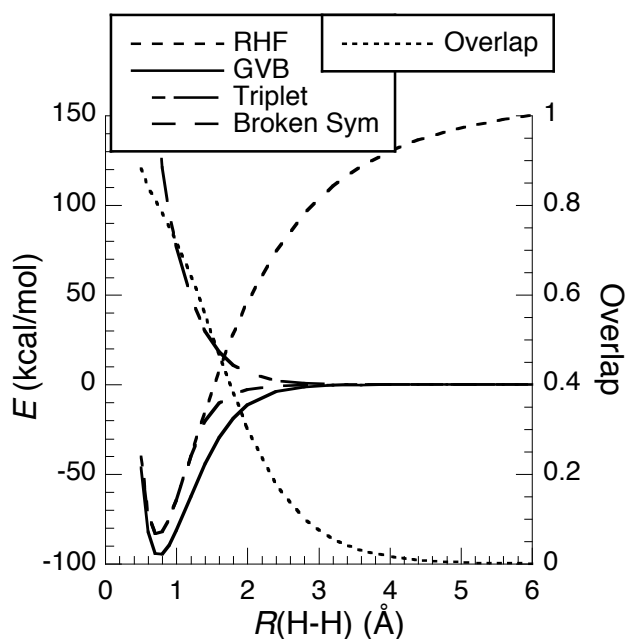


Figure A.1: H₂ dissociation curve in terms of total energy in kcal/mol and GVB overlap

$$S = \frac{c_1 - c_2}{c_1 + c_2} \quad (\text{A.19})$$

is also provided in Figure A.1. The overlap is around 0.8 at the equilibrium R_{HH} distance and smoothly drops to zero as the bond breaks. In contrast the RHF model, ψ_{S_1} in Eq. (A.9), rises above the atomic limits, dissociating into equal parts ionic and covalent. The energy of the repulsive triplet state, ψ_T in Eq. (A.10), rises as R_{HH} decreases. At short distance the energy of the broken symmetry model, Eq. (A.17) or (A.18), tracks the energy of the RHF model. At about 1.5 Å it deviates from the RHF model and dissociates into two hydrogen atoms. This separation point is referred to as the Coulson-Fischer point.⁶ As discussed in Chapter II, the energies of broken symmetry/single determinant models and high-spin descriptions can be combined to

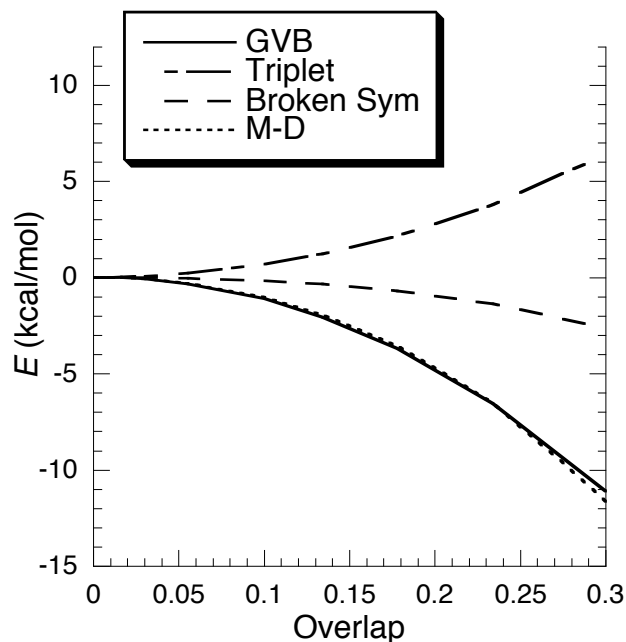


Figure A.2: H₂ molecule total energy as a function of overlap.

obtain estimates for proper multi-determinant spin models of multiplets. This is illustrated in Figure A.2 where the binding energy for GVB, triplet, broken symmetry, and F-D models of H₂ are plotted versus overlap, for the small overlap region. Relative to the GVB model, the single determinant broken symmetry model underestimates the binding energy of the singlet state, whereas the F-D model tracks the GVB description.

REFERENCES

- (1) Ziegler, T.; Rauk, A.; Baerends, E. J. *Theor. Chim. Acta* **1977**, *43* (3), 261–271.
- (2) Noodleman, L.; Davidson, E. R. *Chem. Phys.* **1986**, *109* (1), 131–143.
- (3) Soda, T.; Kitagawa, Y.; Onishi, T.; Takano, Y.; Shigeta, Y.; Nagao, H.; Yoshioka, Y.; Yamaguchi, K. *Chem. Phys. Lett.* **2000**, *319* (3), 223–230.
- (4) Frank, I.; Hutter, J.; Marx, D.; Parrinello, M. *J. Chem. Phys.* **1998**, *108* (10), 4060–4069.
- (5) Noodleman, L. *J. Chem. Phys.* **1981**, *74* (10), 5737–5743.
- (6) Ellis, J. K.; Martin, R. L.; Scuseria, G. E. *J. Chem. Theory Comput.* **2013**, *9* (7), 2857–2869.

APPENDIX B: FD-DFT INTERDETERMINANT DFT EXCHANGE ENERGY FOR FOUR
OPEN SHELL ORBITALS

As mentioned in chapter II, the case of four open shell electrons is special because the configuration only has three unique double spin flips when six unique spin flipped determinants are needed. However, using the four single spin flips, it is possible to solve for the six DFT exchange energies that couple the four open shell orbitals. The eight unique DFT energy determinants are:

$$\begin{aligned}
 E_{\text{DFT,HS}(4)} &= K_{\text{closed}} + K_{1,2} + K_{1,3} + K_{1,4} + K_{2,3} + K_{2,4} + K_{3,4} \\
 E_{\text{DFT},1(4)} &= K_{\text{closed}} + K_{2,3} + K_{2,4} + K_{3,4} \\
 E_{\text{DFT},2(4)} &= K_{\text{closed}} + K_{1,3} + K_{1,4} + K_{3,4} \\
 E_{\text{DFT},3(4)} &= K_{\text{closed}} + K_{1,2} + K_{1,4} + K_{2,4} \\
 E_{\text{DFT},4(4)} &= K_{\text{closed}} + K_{1,2} + K_{1,3} + K_{2,3} \\
 E_{\text{DFT},1,2(4)} &= K_{\text{closed}} + K_{1,2} + K_{3,4} \\
 E_{\text{DFT},1,3(4)} &= K_{\text{closed}} + K_{1,3} + K_{2,4} \\
 E_{\text{DFT},1,4(4)} &= K_{\text{closed}} + K_{1,4} + K_{2,3}
 \end{aligned} \tag{B.1}$$

where $E_{\text{DFT,HS}(4)}$ is the high spin DFT exchange/correlation energy, $E_{\text{DFT},i(4)}$ is the exchange/correlation energy for a single spin flip of orbital i , $E_{\text{DFT},i,j(4)}$ is the exchange/correlation energy for a double spin flip of orbitals i and j , K_{closed} is all exchange/correlation energies between the core orbitals, and $K_{i,j}$ is the exchange/correlation energy between orbitals i and j .

Subtracting the high spin determinant from all spin flip determinants in Eq. (B.1) gives:

$$\begin{aligned}
E_{DFT,HS(4)} - E_{DFT,1(4)} &= K_{1,2} + K_{1,3} + K_{1,4} \\
E_{DFT,HS(4)} - E_{DFT,2(4)} &= K_{1,2} + K_{2,3} + K_{2,4} \\
E_{DFT,HS(4)} - E_{DFT,3(4)} &= K_{1,3} + K_{2,3} + K_{3,4} \\
E_{DFT,HS(4)} - E_{DFT,4(4)} &= K_{1,4} + K_{2,4} + K_{3,4} \\
E_{DFT,HS(4)} - E_{DFT,1,2(4)} &= K_{1,3} + K_{1,4} + K_{2,3} + K_{2,4} \\
E_{DFT,HS(4)} - E_{DFT,1,3(4)} &= K_{1,2} + K_{1,4} + K_{2,3} + K_{3,4} \\
E_{DFT,HS(4)} - E_{DFT,1,4(4)} &= K_{1,2} + K_{1,3} + K_{2,4} + K_{3,4}
\end{aligned} \tag{B.2}$$

This leaves seven equations for six unknowns. The system of equations is overdetermined, so we have chosen to combine the single spin flips in the most symmetric form possible:

$$\begin{aligned}
E_{DFT,HS-1(4)} &= K_{1,2} + K_{1,3} + K_{1,4} \\
E_{DFT,HS-2(4)} &= K_{1,2} + K_{2,3} + K_{2,4} \\
E_{DFT,HS-3(4)} &= K_{1,3} + K_{2,3} + K_{3,4} \\
E_{DFT,HS-4(4)} &= K_{1,4} + K_{2,4} + K_{3,4} \\
E_{DFT,C_1} &= E_{DFT,HS-1(4)} + E_{DFT,HS-2(4)} - E_{DFT,HS-3(4)} - E_{DFT,HS-4(4)} \\
E_{DFT,C_2} &= E_{DFT,HS-1(4)} - E_{DFT,HS-2(4)} + E_{DFT,HS-3(4)} - E_{DFT,HS-4(4)} \\
E_{DFT,C_3} &= E_{DFT,HS-1(4)} - E_{DFT,HS-2(4)} - E_{DFT,HS-3(4)} + E_{DFT,HS-4(4)} \\
E_{DFT,C_1} &= 2K_{1,2} - 2K_{3,4} \\
E_{DFT,C_2} &= 2K_{1,3} - 2K_{2,4} \\
E_{DFT,C_3} &= 2K_{1,4} - 2K_{2,3}
\end{aligned} \tag{B.3}$$

where $E_{DFT,HS-i(4)}$ is the difference between the high spin energy determinant with the single spin flip determinant for orbital i from Eq. (B.2) and E_{DFT,C_j} is the j^{th} single spin flip combination.

Combining the three single spin flip combinations, E_{DFT,C_j} , from Eq. (B.3) with the three double spin flip determinant energies, $E_{DFT,HS-i,j(4)}$, from Eq. (B.2) gives a set of six equations for the six unknown interdeterminant DFT exchange energies.

$$\begin{aligned}
E_{\text{DFT},C_1} &= 2K_{1,2} && -2K_{3,4} \\
E_{\text{DFT},C_2} &= & 2K_{1,3} && 2K_{2,4} \\
E_{\text{DFT},C_3} &= && 2K_{1,4} - 2K_{2,3} && \\
E_{\text{DFT,HS-1,2(4)}} &= & K_{1,3} + K_{1,4} + K_{2,3} + K_{2,4} && \\
E_{\text{DFT,HS-1,3(4)}} &= K_{1,2} & + K_{1,4} + K_{2,3} & + K_{3,4} \\
E_{\text{DFT,HS-1,4(4)}} &= K_{1,2} + K_{1,3} & & + K_{2,4} + K_{3,4}
\end{aligned} \tag{B.4}$$

The equations are linearly independent. These equations are solved via matrix inversion to obtain the individual exchange energies for four open shell orbital multiplet systems.